

18 **Abstract**

19 Bimodal runoff behavior, characterized by two distinct peaks in flow response, often leads to
20 significant stormflow and associated flooding. Understanding and characterizing this phenomenon
21 is crucial for effective flood forecasting. However, this runoff behavior has been understudied and
22 poorly understood in semi-humid regions. In this study, we investigated the response
23 characteristics and occurrence conditions of bimodal hydrograph based on the hydrometric and
24 isotope data spanning 10 years in a semi-humid forested watershed in North China. The main
25 findings include: 1) the onset of the bimodal hydrograph exhibits a threshold behavior, with
26 delayed streamflow peaks occurring when the sum of event rainfall (P) and antecedent soil
27 moisture index prior to the rainfall (ASI) exceeds 200 mm; 2) isotopic hydrograph separation
28 reveals that delayed stormflow process is primarily driven by pre-event water, with increasing
29 contributions of pre-event water during catchment wetting-up; 3) the dynamic variation in
30 groundwater level precedes that of streamflow, establishing a hysteretic relationship wherein
31 groundwater level peaks before streamflow during delayed stormflow. These findings, supported
32 by onsite observations, emphasize the dominance of shallow groundwater flow in the generation
33 of delayed stormflow.

34 **Keywords:** Semi-humid watershed, Stormflow, Bimodal runoff response, Threshold, Shallow
35 groundwater

36 **1. Introduction**

37 Runoff generation is one of the most complex hydrological processes due to their complexity
38 and non-linearity (McDonnell *et al.*, 2007; McGuire & McDonnell, 2010; Phillips, 2003). At

39 different times of a year, the activation of different runoff generating mechanisms, and contrasting
40 compartments and flow routes form different hydrograph shapes, which are generally classified as
41 unimodal and bimodal response types (Jenkins *et al.*, 1994; Gu, 1996; Kosugi *et al.*, 2011). A
42 unimodal response is characterized by a needle-shaped peak which responds immediately to the
43 rainfall impulse. In contrast, the bimodal response contains a delayed damped arch-shaped peak
44 responding to the same rainfall impulse in addition to the direct peak (Martínez-Carreras *et al.*,
45 2016). Generally, the delayed peak in a bimodal event contributes substantially more runoff than
46 the first peak (Zillgens *et al.*, 2007). For instance, the study by Onda *et al.* (2001) showed that the
47 delayed peak discharge is five to ten times greater than the first peak. When the bimodal runoff
48 event occurs, the streamflow increases markedly and lasts for several days. Therefore,
49 characterizing the bimodal response is of great significance to understanding the runoff generation
50 process and essential to achieving improved forecasting of extreme floods.

51 Since the bimodal hydrograph was accidentally observed in Côte d'Ivoire in 1960 during flood
52 frequency analysis and surface runoff generation study (Dubreuil, 1960, 1985), bimodal response
53 has piqued the interest of many hydrologists worldwide and been recorded in watersheds with
54 varied geological and climate conditions. For example, Onda *et al.* (2001) observed bimodal
55 hydrographs in a steep mountainous watershed underlain by shale and serpentinite in Japan (annual
56 precipitation: 1800 mm). Padilla *et al.* (2014, 2015) found delayed peaks after the rainfall in a
57 steep headwater catchment underlain by fractured bedrock also in Japan (annual precipitation:
58 2669 mm). Zillgens *et al.* (2007) recorded a delayed peak after the direct peak in Saalach basin in
59 the Austrian Alps (annual precipitation: 1400 mm). Masiyandima *et al.* (2003) found bimodal
60 responses in an inland valley watershed with wet lowlands in central Côte d'Ivoire (annual rainfall:
61 1045 mm). Anderson and Burt (1977, 1978) observed delayed peak after the storm at Bicknoller

62 Combe in Sommerset, composed of impermeable Old Red Sandstone. The characteristics and
63 conditions of occurrence of bimodal hydrograph can provide an effective method for simplifying
64 the description of complex hydrological systems, and comparing stormflow generation mechanism
65 in different watersheds (Tromp-van Meerveld & McDonnel, 2006). However, most of these studies
66 mentioned above have been done in humid regions with rainfall of more than 1000 mm. To the
67 best of authors' knowledge, very few studies if not none have been conducted in semi-humid
68 environment with rainfall less than 800 mm.

69 Meanwhile, recognizing the pivotal role of bimodal response in runoff generation, researchers
70 have made concerted efforts over the past several decades to quantify its characteristics and
71 establish statistical metrics for identifying the occurrence of bimodal events. Findings suggest that
72 indicators for bimodal response encompass factors such as rainfall amount (Haga *et al.*, 2005),
73 pre-event streamflow (Graeff *et al.*, 2009), soil moisture (Anderson & Burt, 1978; Weyman, 1970),
74 groundwater level (Padilla *et al.*, 2015) and storage (Martínez-Carreras *et al.*, 2016). Taking the
75 work of Martínez-Carreras *et al.* (2016) as an illustrative example, it revealed that the delayed peak
76 manifested only when the watershed storage reached a critical threshold of 113 mm. It is
77 noteworthy that predictors vary significantly among watersheds, with only a limited number of
78 studies presenting quantitative results akin to those reported by Martínez-Carreras *et al.* (2016).
79 Moreover, response timing metrics such as response lag to peak—providing insights into different
80 aspects of water travel time during an event—have received comparatively less attention in the
81 evaluation of threshold effects (Dingman, 2015; Ross *et al.*, 2021).

82 Many studies have delved into the compartments and flow pathways responsible for
83 generating distinct runoff response patterns. The first runoff peaks are attributed to factors such as
84 rainwater directly falling onto the stream channel, rapid flow through preferential paths (Becker

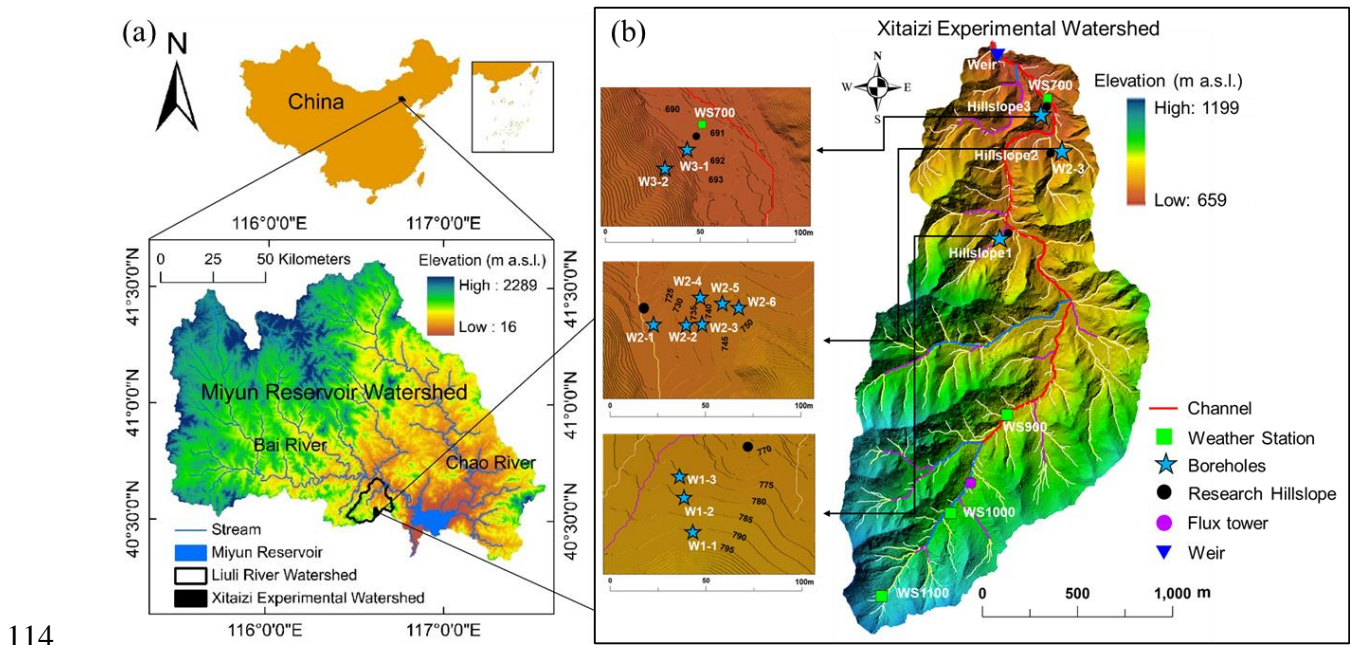
85 & McDonnell, 1998; Martínez-Carreras *et al.*, 2015; Wrede *et al.*, 2015), or saturation-excess
86 overland flow in the riparian zone (Anderson & Burt, 1978; Westhoff *et al.*, 2011). While delayed
87 runoff peaks in bimodal events are primarily linked to subsurface flow processes (Weyman, 1970;
88 Onda *et al.*, 2006; Zillgens *et al.*, 2007; Graeff *et al.*, 2009; Padilla *et al.*, 2015). However, a notable
89 gap exists in the literature, as many studies have focused solely on water flow processes within the
90 soil profile without thoroughly investigating whether subsurface stormflow originates from the
91 soil layer, bedrock layer, or a combination of both.

92 Bimodal responses, representing the nonlinear interplay between runoff and rainfall,
93 inherently showcase the stormflow process in terms of both response timing and magnitude. This
94 intuitive manifestation holds significant implications for advancing runoff modeling (Graeff *et al.*,
95 2009; McDonnell *et al.*, 2007) and enhancing the precision of flash flood forecasting (Zhang *et al.*,
96 2021; Zillgens *et al.*, 2007). In our present study, spanning the years 2014 to 2023, we collected
97 data on rainfall, groundwater levels, soil water content, and streamflow within a semi-humid forest
98 experimental watershed in North China. Our investigation involves characterizing the response
99 magnitude and timing of stormflow to rainfall through hydrograph analysis, while also scrutinizing
100 the composition of the water sources contributing to stormflow. Specifically, we hypothesize that
101 (1) the occurrence of bimodal streamflow responses exhibits a threshold behavior with rainfall and
102 watershed wetness, and (2) the primary source of water for the delayed stormflow is subsurface
103 flow.

104 **2. Materials and Methods**

105 **2.1 Study area**

106 The study headwater catchment, the Xitaizi Experimental Watershed (XEW), is situated at
107 coordinates 40°32'N and 116°37'E, as depicted in Figure 1. Spanning an area of 4.22 km², XEW
108 exhibits elevations ranging from 676 to 1201 m above sea level. Approximately 54% of the area
109 features a slope between 20% and 40%. The region experiences a monsoon-influenced semi-humid
110 climate characterized by an average annual rainfall of 625 mm. The majority of this precipitation,
111 around 80%, occurs between June and September. The annual mean temperature in the area is
112 11.5°C, accompanied by a relative humidity of 59.1%. Experimental and observational activities
113 were conducted over the period from 2014 to 2023.



115 **Figure 1.** Location of the Xitaizi Experimental Watershed (XEW) in North China (a), and the
116 detailed distributed monitoring stations and instruments (b), including four automatic weather
117 stations (WS700-1100), one weir, and eleven groundwater boreholes (blue star corresponds with
118 well numbers and locations). Four rain gauges are located near the weather stations, and one is
119 located adjacent to the weir.

120

121 XEW represents a typical location in North China's earth-rocky mountainous region, where
122 approximately 80% of the catchment area is underlain by firmly compacted, deeply weathered
123 granite. Soil mapping and field investigations reveal the prevalent soil types to be brown earth and
124 cinnamon soil (according to Chinese soil taxonomy), with a depth extending to 1.5 meters. The
125 saturated hydraulic conductivity of the soil ranges from 19.5 to 175.3 mm/h, with an average value
126 of 45 mm/h. The bedrock in the area is primarily composed of granite, constituting approximately
127 88% of the total bedrock composition, while gneiss and dolomite are sporadically distributed.
128 Some sections of the granite exhibit fracture, and a layer of regolith is sandwiched between the
129 soil layer and the bedrock layer. In terms of land cover, the catchment is predominantly covered
130 by forest (98%), with 54.2% being broad-leaved, 2.3% coniferous, and 10.5% a mix of coniferous
131 and broad-leaved. The remaining 33% consists of shrubs (Tie *et al.*, 2017).

132 **2.2 Meteorology and runoff measurements**

133 Meteorological variables and runoff have been systematically monitored since 2013.
134 Meteorological conditions were consistently measured using four GRWS100 automatic weather
135 stations ~~(Campbell Scientific, Inc., Logan, UT, USA)~~. These weather stations were strategically
136 distributed quasi-uniformly along the elevation gradient, as depicted in Figure 1. The
137 comprehensive data collection from these stations contributes to a thorough understanding of the
138 meteorological dynamics in the study area over the specified timeframe.

139 For the measurement of air temperature (T_a) and relative humidity at each automatic weather
140 station, an HC2S3-L temperature and relative humidity probe (~~Rotronic AG, Grindelstrasse,~~
141 ~~Bassersdorf, Schweiz~~) was utilized. These probes were equipped with a radiation shield to enhance
142 accuracy. Simultaneously, a LI-190R quantum sensor (~~LI-COR, Inc., Lincoln, NE, USA~~) was
143 employed to measure photosynthetically active radiation (PAR). Rainfall data were collected at
144 10-minute intervals using six tipping-bucket rain gauges (~~Texas Electronics, Inc., Dallas, TX,~~
145 ~~USA~~). These gauges were positioned in an open space near the automatic weather stations, and
146 average values were adopted for analysis in this study.

147 Furthermore, the antecedent precipitation index (API), generally used to represent the residual
148 effect of previous precipitation (Mosley, 1979; Iwagami *et al.*, 2010), was calculated for all the
149 events over 3, 6, and 12 days. The API during the antecedent t days is described as follows:

$$150 \quad \text{API}(t) = \sum_{i=1}^t \frac{P_i}{i} \quad (1)$$

151 where i is the day count and P_i is the daily precipitation in the i^{th} day previously.

152 A Parshall flume was installed at the catchment outlet to measure streamflow (Figure 1). The
153 water level in the flume was measured every 5 min with a HOBO capacitance water level logger
154 (~~Onset, Bourne, Massachusetts, USA~~) from 2014. Streamflow was calculated using the standard
155 Parshall flume rating curve, and both the rainfall and streamflow measurements were averaged to
156 hourly timesteps, and in this study, the analysis is conducted at hourly timesteps. Unfortunately,
157 the observation equipment is susceptible to failures due to the complex environmental conditions
158 and disturbances caused by wild animals and plants. Compounded by the remote location of XEW,
159 accessing the site promptly to address malfunctions is challenging, leading to the loss of some
160 observation data. Notably, stormflow data from July 19 to August 16, 2016, had to be excluded

161 because the road collapsed during a heavy storm, preventing a significant amount of runoff from
 162 passing through the Parshall flume. Furthermore, streamflow data from 2018 to 2019 are
 163 unavailable, and the two bimodal events in 2016 were omitted from the hysteresis analysis due to
 164 substantial errors in streamflow observations resulting from damage to the diversion channel. The
 165 specific observation periods are detailed in Table 1. These limitations underscore the challenges
 166 associated with conducting observations in remote and environmentally intricate locations.

167 **Table 1.** Rainfall-runoff event classification and counts by Year. This table provides a
 168 breakdown of the number of rainfall-runoff events categorized as unimodal, bimodal, and hybrid
 169 bimodal for each year, along with the corresponding time periods. The total counts are
 170 summarized at the bottom.

Year	Unimodal event	Bimodal event	Hybrid bimodal event	Time period
<u>Characteristics</u>	<u>A needle-shaped peak which responds immediately to the rainfall impulse</u>	<u>A delayed damped arch-shaped peak responding to the same rainfall impulse in addition to the direct peak</u>	<u>The delayed peak increased rapidly and merged with the direct peak, generating extremely high streamflow volume</u>	
2014	7	-	-	Jul 25 - Sep 25
2015	12	2	-	Jun 1 - Oct 1
2016	2	2	1	Jul 10 - Aug 20
2017	-	2	-	Jun 20 - Jul 10
2020	14	2	-	Jul 1 - Oct 10
2021	15	5	2	Jun 1 - Oct 10
2022	18	1	-	Apr 1 - Nov 1
2023	9	-	1	Apr 1 - Nov 1
Total	77	14	4	

171

172 **2.3. Soil water content observation**

173 Volumetric soil water content (SWC) was measured at eight observation sites using CS616
 174 time-domain reflectometry (TDR) probes (~~Campbell Scientific, Inc., Logan, UT, USA~~) at 10-min
 175 intervals. These measurements were taken at 10-minute intervals. On Hillslope 1, five soil
 176 moisture sensors were deployed, with an additional three located adjacent to WS900. These

177 sensors were strategically placed in the soil profiles at 80 cm depth intervals, each at a depth of 10
178 cm. For analysis in this study, the 10-minute interval measurements were aggregated to hourly
179 time steps, and the arithmetic mean of the total SWC across the four profiles was employed.
180 Moreover, SWC data immediately preceding a rainfall event were integrated over the 80 cm depth
181 to calculate an antecedent soil moisture index (ASI), as proposed by Haga *et al.* (2005). This index,
182 commonly utilized in analyzing the impact of antecedent shallow soil water storage on catchment
183 runoff response (Fu *et al.*, 2013; Penna *et al.*, 2011), provides valuable insights into the soil
184 moisture conditions preceding rainfall events.

185 **2.4 Groundwater level observation**

186 Fluctuations in groundwater level (below the ground surface, hereinafter referred to as bgs)
187 were systematically recorded in eleven 80 mm diameter boreholes situated on three hillslopes
188 within the catchment (refer to Figure 1). The boreholes were drilled to depths of 5-26 m in granite
189 (weathered and fractured to varying extents) mantled by thin soils. Unscreened portions of the
190 boreholes accounted for approximately one third to three fifths of the total depth (refer to Table 2).
191 To capture the groundwater level dynamics, HOBO capacitance water level loggers (Onset, USA)
192 were deployed to record water levels in the boreholes at hourly intervals. It is noteworthy that
193 water levels were rarely observed in boreholes W1-1, W1-2, W2-4, W2-5, and W2-6. This
194 observation could be attributed to the boreholes potentially not being drilled deep enough to reach
195 the groundwater, possibly due to challenges encountered during field drilling. Slug tests conducted
196 following installation suggested that the saturated conductivity in the weathered and fractured
197 granite was relatively high, ranging from 5.2×10^{-3} m/day to as high as 1.16 m/day.

198 **Table 2.** Depths and ~~Groundwater-groundwater Levels-levels~~ of ~~B~~boreholes. This table
 199 summarizes the depths of the bottom and the boundary between unscreened and screened portions,
 200 along with the shallowest and deepest groundwater levels of boreholes in the study area.

Borehole	Bottom (m)	Boundary (m)	Shallowest GWL (m)	Deepest GWL (m)
W1-3	10	6	2.8	10 ^a
W2-1	5	2	0.2	2.2
W2-2	10	4	4.8	10 ^a
W2-3	26	9	6.4	12.2
W3-1	10	4	0.8	3.9
W3-2	10	4	6.1	9.9

201 Note: All values indicate depths (in meters) from the ground surface; GWL represents groundwater
 202 level; 'a' indicates the groundwater level dropped below the bottom of the borehole.
 203

204 An index for groundwater level (I_G) was computed by normalizing the groundwater levels in
 205 each borehole to their recorded range throughout the research years, following the approach
 206 outlined by Detty and McGuire (2010). Subsequently, the arithmetic mean of I_G across all
 207 boreholes was calculated, serving as a representative proxy for the groundwater level across the
 208 entire catchment. This approach provides a standardized measure that allows for the comparison
 209 of groundwater level variations across different boreholes within the study area.

210 **2.5 Separation of rainfall-runoff events**

211 An intensity-based automatic algorithm, as outlined by Tian *et al.* (2012) and Powell *et al.*
 212 (2007), was employed to delineate and segregate rainfall events from hourly rainfall time series
 213 data. In this algorithm, a threshold rainfall intensity of >0.1 mm/h was utilized to determine the
 214 commencement and conclusion of each event, with individual storms being separated by a
 215 minimum of six hours. Events characterized by an accumulated rainfall exceeding 5 mm were
 216 selected for further analysis. A total of 95 distinct rainfall events, each with a cumulative rainfall
 217 of at least 5 mm, were identified and isolated from the rainfall data series spanning the years 2014
 218 to 2023, employing the intensity-based automatic method (refer to Table 1).

219 Storm runoff events are identified when streamflow experiences a rapid increase and attains
220 a peak in response to a rain impulse. Throughout the analyses presented, streamflow refers to the
221 total discharge measured at the weir. The computer program HYSEP (Sloto & Crouse, 1996) was
222 employed to automatically partition a streamflow hydrograph into baseflow and stormflow
223 components. Subsequently, the automated separation outcomes underwent manual verification and
224 adjustment, aligning with observed data and widely accepted straight-line separation
225 principles.~~The separation of stormflow from base flow was achieved using the straight line~~
226 ~~separation method, as illustrated in Figure 2. This method involves drawing a line from the~~
227 ~~hydrograph's initial climb to the point of inflection on the recession limb, following the approach~~
228 ~~outlined by Zillgens *et al.* (2007).~~ In the context of each event, q_0 is defined as the streamflow
229 before the onset of rainfall. This parameter characterizes the baseflow conditions preceding the
230 hydrograph's response to a rain impulse (Zillgens *et al.*, 2007). The separation of stormflow from
231 base flow allows for a more detailed examination of the runoff dynamics during distinct rainfall
232 events.

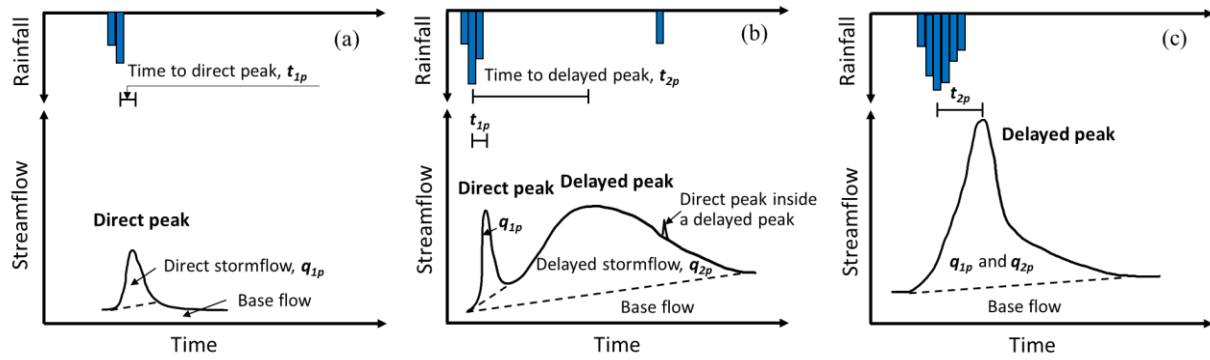
233 **2.6 Hydrograph and event types**

234 The hydrograph served as a valuable tool for characterizing the timing, magnitude, and
235 duration of runoff responses to rainfall. Two primary response types were identified based on the
236 number and shape of streamflow peaks: unimodal and bimodal events. Schematic diagrams
237 illustrating these three types of events are presented in Figure 2.

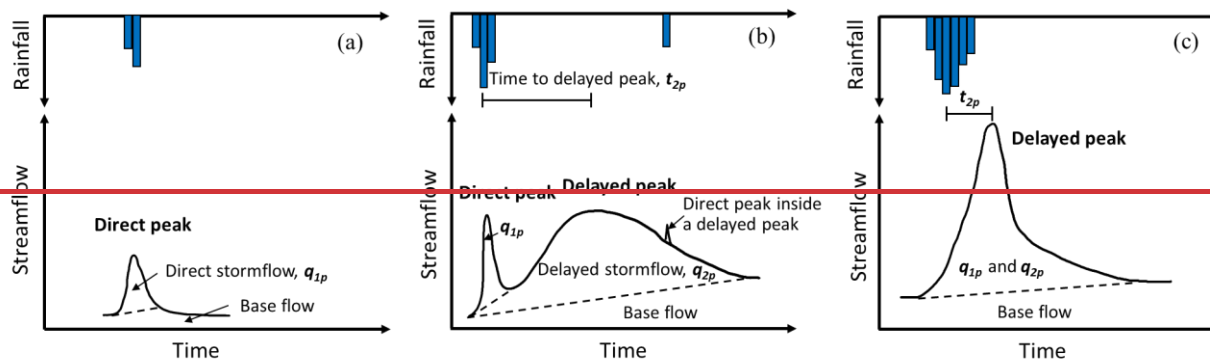
238 A unimodal event has a single peak generates during or shortly after the cessation of rain
239 impulse (refer to Figure 2a). While a bimodal event features two peaks as a response to the same
240 rain impulse, of which the direct peak (also called the first peak) corresponds to a fast catchment
241 response to rainfall and occurs synchronously with the rainfall or shortly after its onset.

242 Additionally, we referred those events has a similarly shaped hydrograph to unimodal event, but
243 the water yield and peak delay time are significantly greater, as hybrid bimodal events.
244 ~~Additionally, a delayed peak appears after the direct peak, exhibiting a pronounced recession that~~
245 ~~can last up to several days. In cases where the delayed peak rapidly merges with the direct peak~~
246 ~~into a single peak, the event is referred to as a hybrid bimodal event.~~ Hybrid bimodal events can
247 be are distinguished from unimodal events by their extremely high streamflow volume, longer
248 duration, and delayed response time (Figure 2c). The hydrographs of bimodal and hybrid bimodal
249 events can refer to Figures 12 and 13.

250 It's worth noting that a rainfall event may consist of multiple impulses, and in such cases, the
251 hydrograph responds with multiple direct peaks (see Figure 2b). The stormflows from the first
252 peak (q_{1p}) and delayed peak (q_{2p}), along with the total event stormflow ($q_s = q_{1p} + q_{2p}$), were
253 calculated by summing hourly values over the identified event period. The runoff ratio (R_r),
254 commonly used to estimate the effective contributing area during a runoff event (Buttle *et al.*, 2004;
255 Detty & McGuire, 2010), is calculated as the ratio of q_s to gross rainfall.



256



257

258 **Figure 2.** Schematic diagrams of the hydrographs of an (a) unimodal event, (b) typical bimodal
 259 events, and (c) hybrid bimodal event (modified from Zillgens *et al.*, 2007).

260

261 **2.7 Definition of lag time**

262 The lag time, defined as the duration between peak rainfall and peak streamflow (Mosley,
 263 1979), is a critical parameter for modeling the temporal variability of streamflow. Lag time varies
 264 significantly among different water sources (Becker, 2005; Haga *et al.*, 2005) and has been
 265 introduced to comprehend sub-components of runoff in different response processes. In this study,
 266 two specific lag times are considered: t_{1p} the time lag between peak rainfall intensity and the first
 267 streamflow peak, and t_{2p} the time lag between peak rainfall intensity and the delayed streamflow
 268 peak, as illustrated in Figure 32.

269 **2.8 Water sampling and isotope analysis**

270 Water samples for isotope analysis ($\delta^{18}\text{O}$ and δD) were collected from July 1 to September 1,
271 2021. Rainwater was automatically sampled every two hours using an ISCO6712 automatic water
272 sampler (Inc., Lincoln, Nebraska, USA) positioned near the weir. Manual bulk samples of rainfall
273 were also collected at the same location after each event using a rainwater sampler with a 9.5 cm
274 diameter funnel attached to a 500 ml plastic water bottle, insulated with bubble foil to protect
275 against direct sunlight, and a table tennis ball placed in the funnel's mouth to minimize evaporation.

276 Stream water was collected every two hours upstream of the Parshall flume location using an
277 automatic water sampler (Figure 1). Spring, seepage water, and groundwater were manually
278 collected daily from boreholes using a bailer. All collected samples underwent isotopic
279 composition analysis ($\delta^{18}\text{O}$ and δD) using a Picarro L2140-i isotopic liquid water and water vapor
280 analyzer (wavelength-scanned cavity ring-down spectroscopy, WS-CRDS) with a declared
281 precision of $\delta^{18}\text{O} \pm 0.1\text{‰}$ and $\delta\text{D} \pm 1\text{‰}$.

282 **2.9 Isotopic hydrograph separation**

283 To trace the source of the streamflow during storm events, a simple mass balance approach
284 was employed to segregate the streamflow into two components: event water and pre-event water.
285 These components are represented by rainfall and baseflow, respectively, based on the oxygen
286 isotopic concentration ($\delta^{18}\text{O}$) of each component. The $\delta^{18}\text{O}$ of baseflow and weighted rainwater
287 samples served as end members, defining the ultimate isotopic composition of the stream, in
288 accordance with the approach outlined by Padilla *et al.* (2014):

289
$$C_s = xC_e + (1 - x)C_p \quad (2)$$

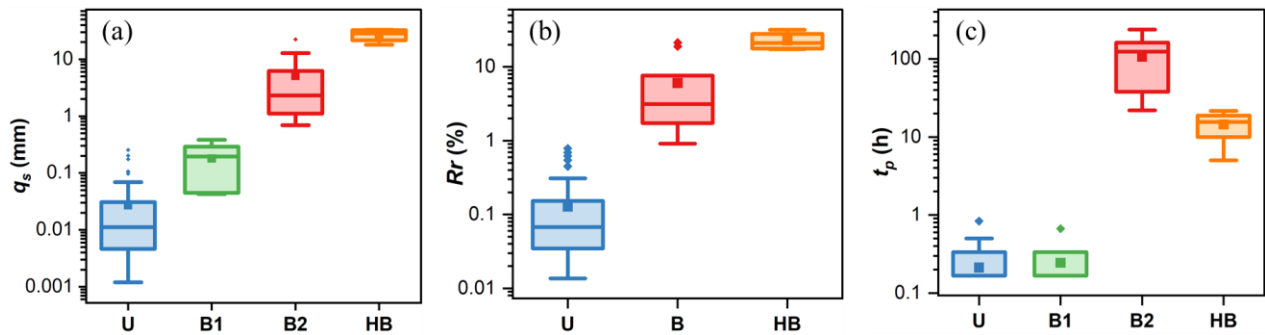
290
$$x = \frac{C_s - C_p}{C_e - C_p} \cdot 100[\%] \quad (3)$$

291 where C_s , C_e and C_p refer to $\delta^{18}\text{O}$ concentrations of stream, event and pre-event water components,
 292 respectively. C_e is the weighted value calculated using the incremental mean weighting method
 293 (McDonnell *et al.*, 1990) for each event. C_p is determined from the stream $\delta^{18}\text{O}$ concentration
 294 measured immediately preceding the rainfall. x is the percentage of event water in stream.

295 3. Results

296 3.1 Characteristics of different runoff response types

297 During the period from 2014 to 2023, a total of 95 distinct rainfall events, each with a
 298 cumulative rainfall of at least 5 mm, were identified from the rainfall data series. Among these
 299 events, 14 exhibited a bimodal response, and an additional 4 displayed a hybrid bimodal process
 300 (refer to Table 1).



301
 302 **Figure 3.** Comparison of (a) stormflow, q_s , (b) runoff ratio, Rr and (c) lag time (t_p) from peak
 303 rainfall to peak streamflow of different event types. U indicates unimodal event, B (including the
 304 first peak B1 and the delayed peak B2) bimodal event and HB hybrid bimodal event. In each
 305 boxplot, the lower and upper limits represent the lower and upper quartiles, while the whiskers
 306 extend to the minimum and maximum values in each dataset. The horizontal line within the box
 307 signifies the median. Individual asterisks denote points more than 1.5 times away from the median.
 308 It's noteworthy that a semi-logarithmic coordinate was utilized for enhanced interpretability due
 309 to the extensive range.

310 The stormflow volume and lag times of streamflow peaks for both unimodal and bimodal
 311 events were determined and characterized. As depicted in Figure 3, unimodal events generated

312 relatively minimal runoff, with a maximum q_{1p} of 0.25 mm. In contrast, the q_{1p} and q_{2p} of bimodal
313 events exhibited a wider range, spanning from 0.03 to 0.38 mm and from 0.82 to 31.63 mm,
314 respectively (Figure 3b). The stormflow volume of bimodal events proved to be 3 to 114 times
315 larger than that of unimodal events, primarily due to the presence of delayed peaks (Figure 3a).
316 Correspondingly, bimodal events displayed higher Rr values ranging from 0.91% to 31.81%,
317 whereas the Rr of unimodal events remained below 0.8% (Figure 3b). This discrepancy suggests
318 an expanded effective contributing area during bimodal and hybrid bimodal events, as highlighted
319 in previous studies (Zhang *et al.*, 2021).

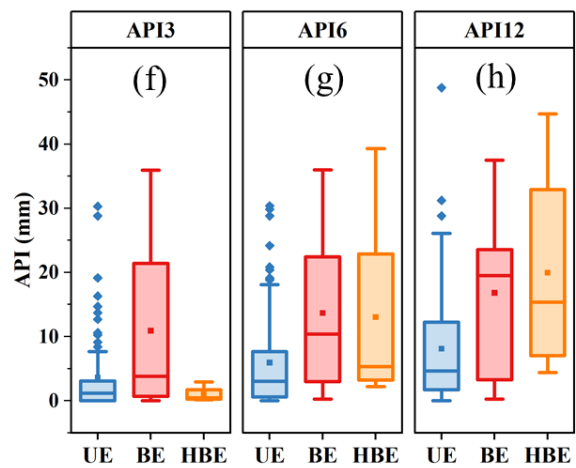
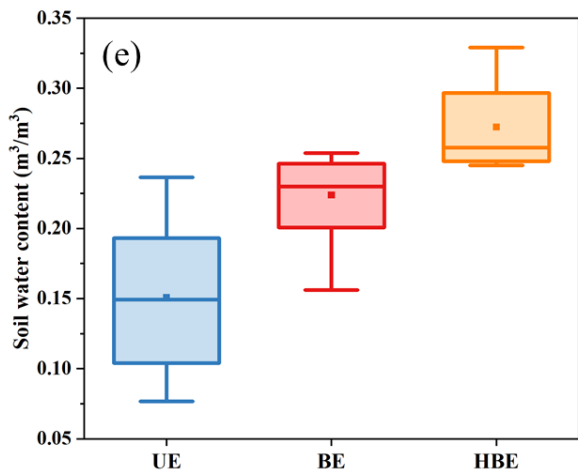
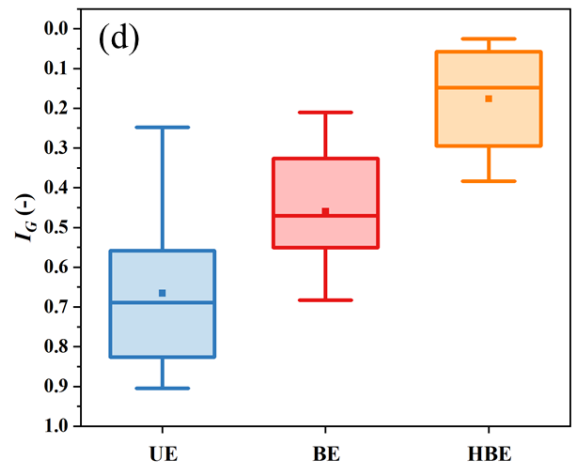
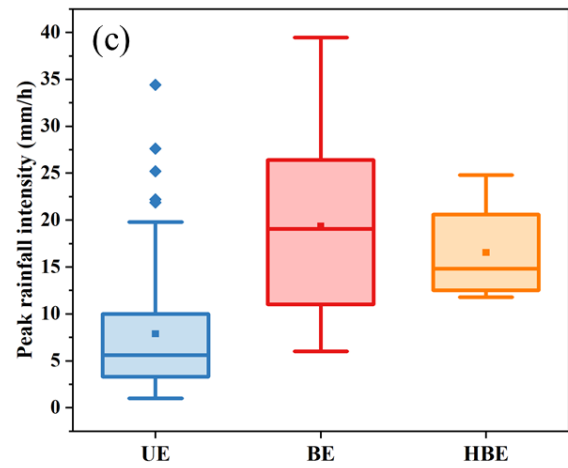
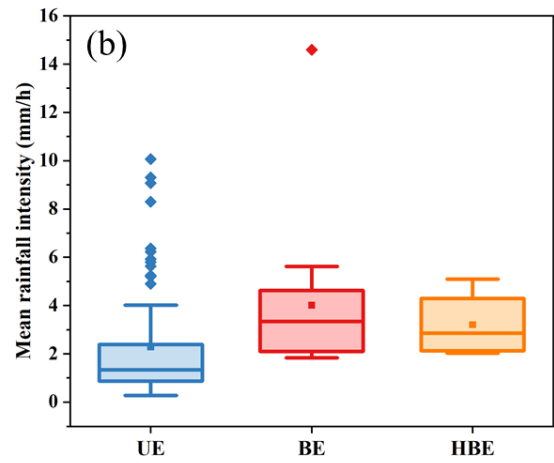
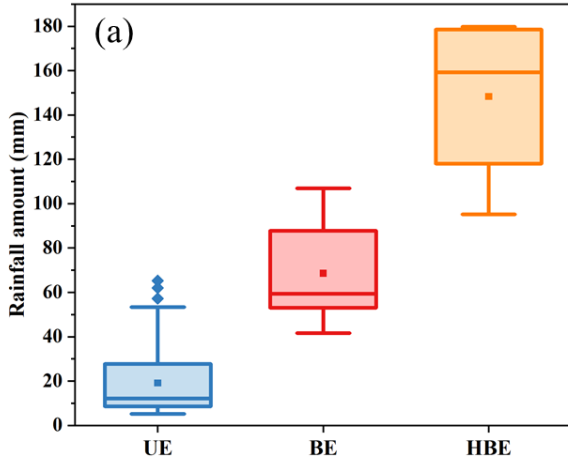
320 In both unimodal and bimodal events, all direct peaks were observed within a one-hour
321 timeframe. However, the delayed peak, a distinctive feature of bimodal events, manifested itself
322 between 5 hours and 9.9 days after the occurrence of the direct peak. Notably, hybrid bimodal
323 events exhibited shorter lag times and significantly higher stormflow yield, underscoring the need
324 for heightened attention in flood forecasting. The substantial difference in lag time strongly implies
325 that these peaks are contributed by distinct water sources, aligning with findings from previous
326 studies (Haga *et al.*, 2005).

327 **3.2 Determinants of delayed streamflow peaks**

328 The relationships between different event types and rainfall characteristic parameters and
329 watershed wetness indicators were further depicted in Figure 4. It is noteworthy that the soil water
330 content (SWC) and groundwater level index (I_G) presented in Figure 4 represent data recorded at
331 the end of rainfall events, considering that delayed streamflow peaks typically manifest subsequent
332 to the cessation of rainfall events. Rainfall amount, ~~groundwater level index (I_G), and soil water~~
333 ~~content (SWC)~~ were statistically significantly different for both groups, as proven by the t-test of
334 equality of medians at a significance level of $\alpha=0.01$. The transition from unimodal to bimodal

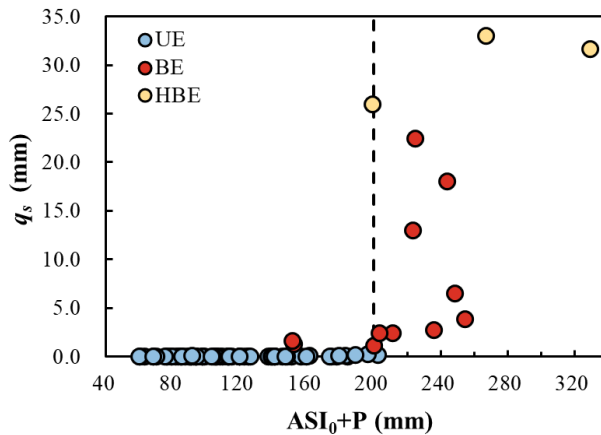
335 events reveals a consistent increase in rainfall amount, I_G , and SWC. Nearly all bimodal events
336 exhibited rainfall amounts exceeding 50 mm, whereas the range for unimodal events varied from
337 5.2 to 66.6 mm (Figure 4a). This suggests that the initiation of delayed streamflow peaks may be
338 associated with substantial rainfall.

339 The I_G and SWC of bimodal events, especially hybrid bimodal events, were significantly
340 higher ($p < 0.01$) than those of unimodal events. Despite partial overlap in the ranges of I_G and
341 SWC for these groups (Figure 4d and e), the mean I_G and SWC values for bimodal events (0.46
342 and 0.67) were notably greater than those for unimodal events (0.22 and 0.13), underscoring the
343 distinctiveness of these parameters between event types. Contrastingly, peak rainfall intensity,
344 mean rainfall intensity, and Antecedent Precipitation Index (API) metrics (API3, API6, and API12)
345 exhibited a widespread overlap in their variation ($p > 0.05$, Figure 4b, d, g-i). Consequently, while
346 bimodal events were characterized by higher rainfall and antecedent wetness, I_G and SWC emerged
347 as more effective indicators for estimating the occurrence of bimodal events, while peak rainfall
348 intensity, mean rainfall intensity, and API were found to be insufficient for distinguishing between
349 bimodal and unimodal events.



351 **Figure 4.** Box plots of the hydrological characteristic parameters for unimodal and bimodal events.
352 (a) rainfall amount; (b) mean rainfall intensity; (c) peak rainfall intensity; (d) I_G : groundwater level
353 index; (e) soil water content; (g)-(i) API3, API6 and API12: antecedent precipitation index over 3,
354 6 and 12 days. UE, BE and HBE are respectively unimodal, bimodal and hybrid bimodal events.
355 To be noted, each element of the box carries the same interpretation as described in Figure 3.

356
357 Considering the interdependence of groundwater level, streamflow, and SWC on rainfall, a
358 detailed examination of the relationship between rainfall amount and bimodal events was
359 conducted. The analysis revealed that the occurrence of delayed peaks is contingent on both event
360 rainfall and antecedent wetness, displaying a distinct threshold behavior (Figure 5b). The
361 combined sum of event rainfall amount (P) and antecedent soil moisture index prior to the rainfall
362 (ASI_0) serves as a reliable indicator for predicting the occurrence of delayed peaks. Figure 5
363 illustrates that bimodal events tend to manifest when $P + ASI_0$ exceeds 200 mm (with only two
364 bimodal events misplaced). An intriguing observation is that these misplaced bimodal events
365 produced very little q_s , and these ~~three~~ unimodal events nearby to the threshold, occurred just
366 before the year's first bimodal response when the watershed was sufficiently humid, signaling a
367 predisposition for bimodal events. However, once the rainfall surpassed the threshold, all bimodal
368 episodes were randomly distributed, and no discernible relationship was observed between their
369 stormflow volume (q_s) and rainfall amount. Based on these findings, we posit that the stormflow
370 generation process may be dominated by groundwater or SWC.



371

372 **Figure 5.** Relationship between the $ASI_0 + P$ and stormflow volumes (q_s) of different event types.
 373 UE is unimodal event, HBE is hybrid bimodal event, P is rainfall amount, and ASI_0 is antecedent
 374 soil moisture index before the rainfall.

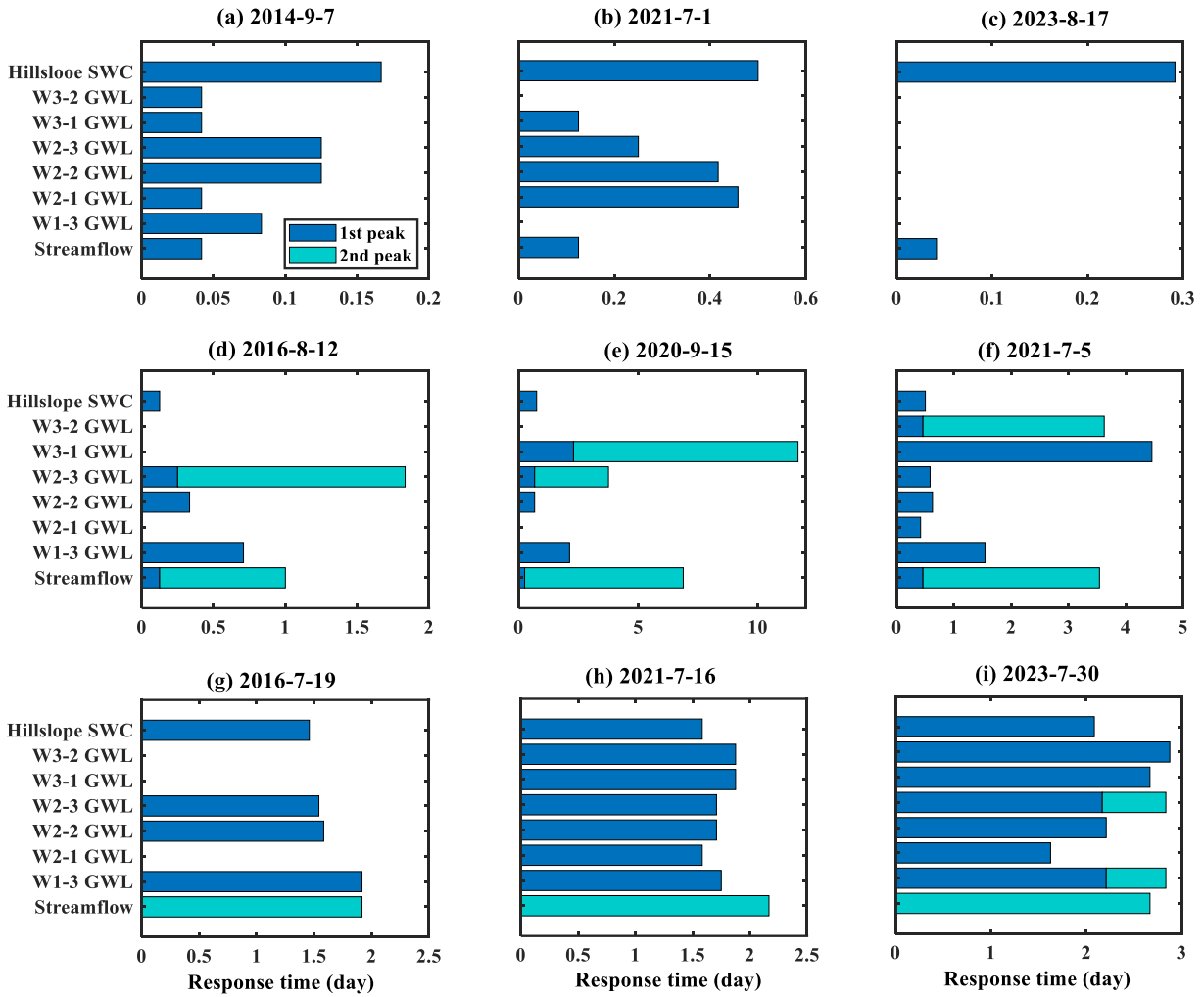
375

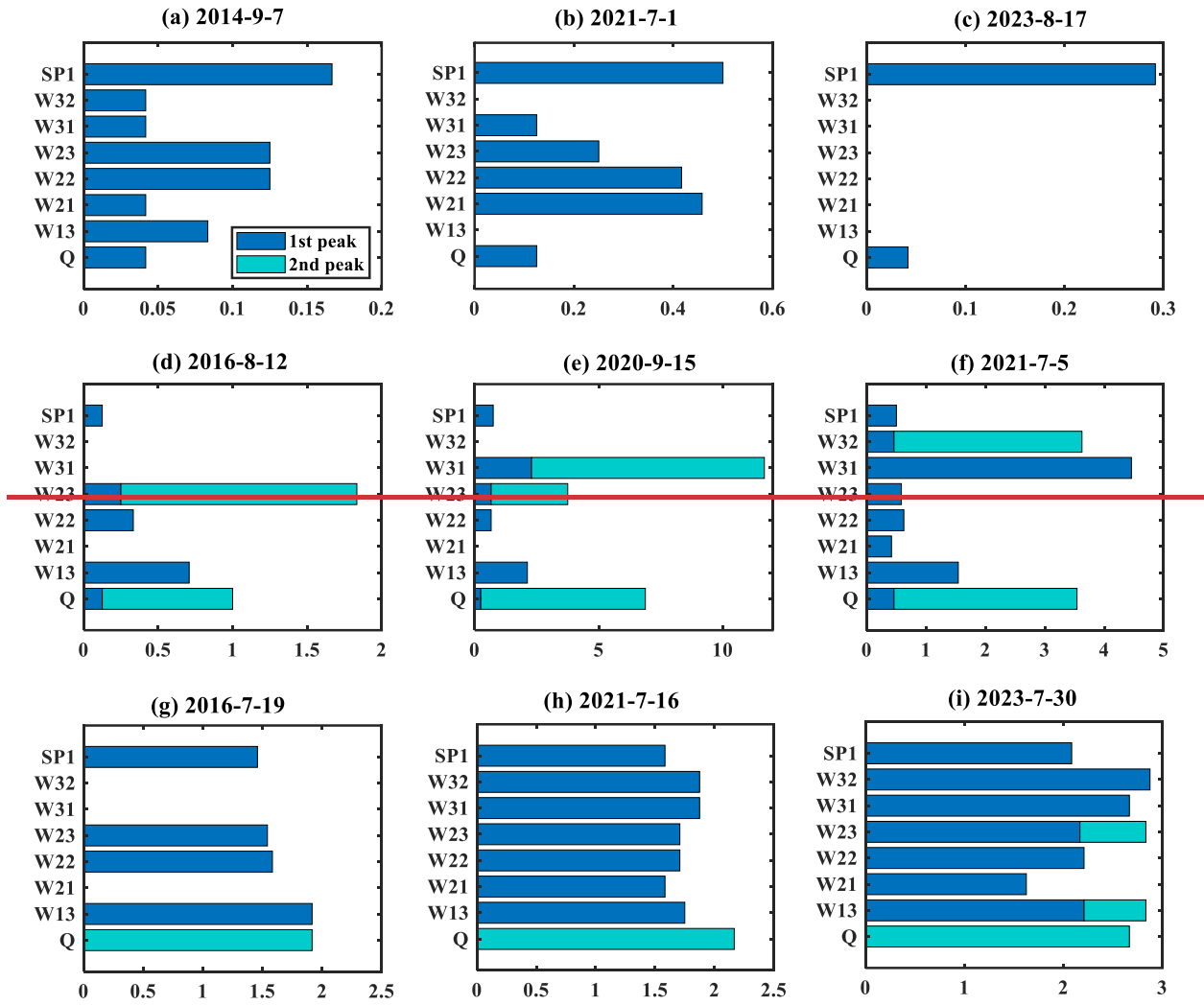
376 3.3 Timing of groundwater, soil water, and streamflow response

377 The preceding analysis indicates a correlation between different event types and groundwater
 378 levels along with SWC. Moreover, the inconsistent response time among different event types may
 379 signify distinct contributing sources to the stream channel, providing insights into the primary
 380 mechanisms behind runoff generation. Earlier or identical response timing of groundwater
 381 compared with streamflow suggested that streamflow response was driven by hillslope
 382 groundwater (Haught and Meerveld, 2011; Rinderer *et al.*, 2016). To explore this further, six
 383 bimodal events with minimal or sporadic rainfall during the delayed peak period, along with three
 384 unimodal events, were selected. The response timing of groundwater, SWC, and streamflow is
 385 illustrated in Figure 6. Each horizontal bar represents the onset of rain on the left end and the lag
 386 time for the peak value on the right end of the corresponding variable. It's worth noting that some
 387 groundwater levels in Figures 6d, e, and g lack horizontal bars due to missing groundwater level

388 data, while the groundwater levels in Figure 6c lack horizontal bars due to no response from
389 groundwater.

390 SWC reached their maximum after direct streamflow peaks but before delayed peaks.
391 Particularly in typical bimodal events, SWCs peaked much earlier than delayed streamflow peaks,
392 suggesting that, in these events, soil water did not contribute to direct peak but may to delayed
393 streamflow peaks. Regarding groundwater levels, some locations showed two peaks and not all
394 responded to the same rainfall event. Among different locations, groundwater levels peaked before
395 or after the delayed streamflow peaks. However, for the hybrid bimodal events, the response time
396 of groundwater levels at various locations, and even the SWC tended to coincide with the delayed
397 streamflow peak. Identical response timing or groundwater rising and peaking just before the
398 stream suggest that whole catchment or critical zone contributed to groundwater may be the major
399 contribution of delayed stormflow.



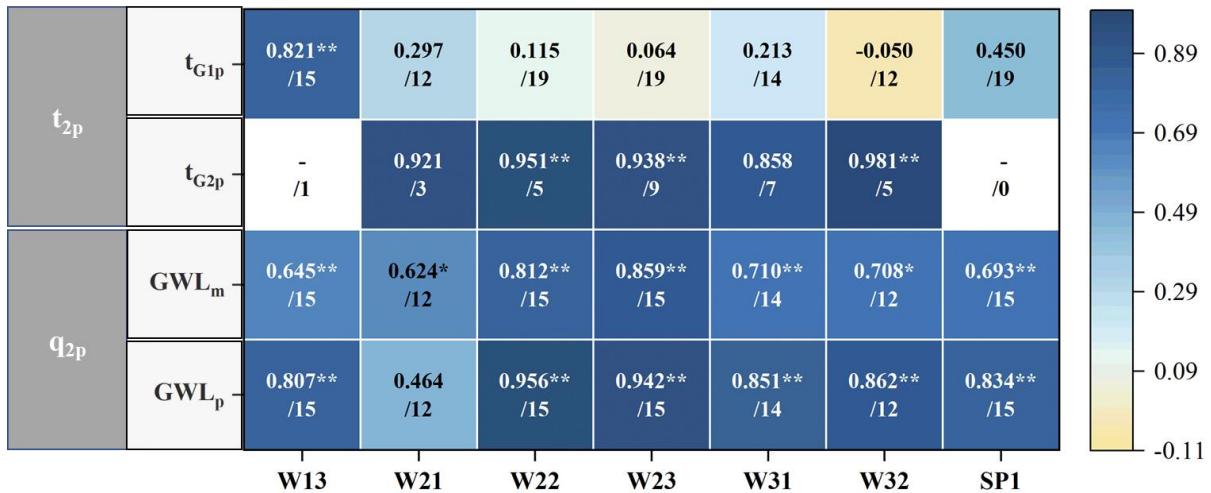


401
 402 **Figure 6.** Response time of streamflow, groundwater level and soil water content in nine events.
 403 The horizontal axis illustrates the lag time from the onset of rainfall. The bar lengths depict the
 404 time taken for volumetric water content and groundwater level to reach their respective maximums
 405 from the onset of rainfall. The horizontal axis represents the lag time from the onset of rain (days).
 406 The lengths of the bars represent the time lag for volumetric water content and groundwater level
 407 to reach the maximums from rainfall onset. GWL is groundwater level, and SWC is soil water
 408 content. Each row and column chart shares identical vertical and horizontal axis titles.

409 Pearson correlation coefficients (r_p) between peak groundwater levels, peak SWC and
 410 delayed streamflow were calculated for 19 bimodal events. As showed in Figure 7, the first two
 411 lines show the correlation coefficients between t_{2p} and the lag time of the peak groundwater levels
 412 and SWC, t_{G1p} and t_{G2p} represent the response times of the first and second peaks of groundwater

413 level or SWC, respectively. The last two lines show the correlation coefficients between q_{2p} and
 414 the average and peak values of groundwater levels and SWC. The number after the slash specifies
 415 how many pairs of the variables.

416 Groundwater levels exhibited two peaks in some events, with the exception of W13.
 417 Correspondingly, among these events, the response time of the second peak of groundwater level
 418 has a strong correlation with t_{2p} with the $r_p > 0.858$. Even though W13's groundwater level only
 419 has one peak, this peak's response time was highly correlated with t_{2p} at the 0.01 significance level
 420 ($r_p = 0.821$). In contrast, SWC displayed one peak in all events, and its response time exhibited a
 421 weak correlation with t_{2p} ($r_p = 0.450$). Both groundwater levels and SWC, particularly their peak
 422 values, demonstrated a high correlation with delayed stormflow volumes (q_s). Above all,
 423 groundwater is deemed to be the primary controlling factor in delayed stormflow.



424

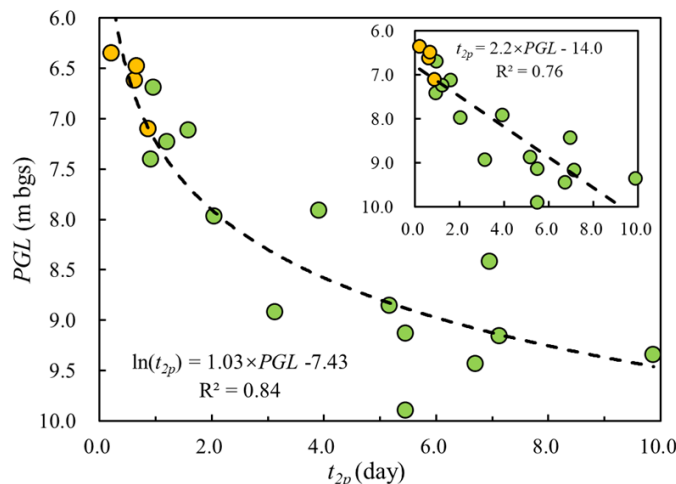
425 Figure 7. Pearson correlation coefficients between peak streamflow and peak groundwater levels.
 426 The number after the slash specifies how many pairs of the variables. IG, groundwater water level
 427 index; ** Denotes that correlation is significant at the 0.01 level (two-tailed).
 428

429 The robust correlation observed between groundwater levels at different locations and
 430 stormflow suggests that groundwater observations at a specific location can serve as a
 431 representative proxy for the overall groundwater level across the watershed. Given the relatively

432 complete and dynamic water level observation data for W23, this borehole was selected for further
433 analysis (Figure 7e).

434 3.4 Stormflow timing and magnitude characteristics

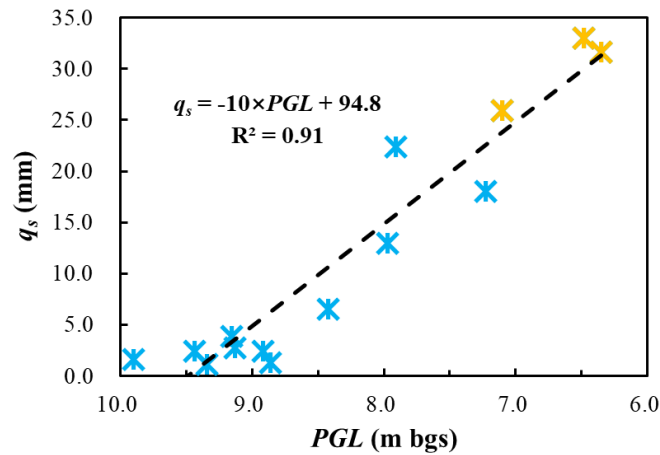
435 Considering the high correlation between streamflow and groundwater level as indicated in
436 the previous analysis, we hypothesized a connection between groundwater and delayed stormflow.
437 To elucidate this correlation between groundwater and streamflow, we fitted the relationship
438 between the groundwater level at location W23 and the magnitude and timing of the delayed
439 stormflow for bimodal events. The time lag of delayed peak (t_{2p}) shows a negative exponential
440 correlation with peak groundwater level ($\ln(t_{2p}) = 1.03 \times PGL - 7.43$, $R^2 = 0.84$, $p < 0.01$, Figure
441 8), suggesting that a higher groundwater level corresponds to a faster response of the delayed
442 runoff peak to rainfall. A comparable linear correlation was also fitted between t_{2p} and groundwater
443 level, albeit with a slightly lower R^2 ($R^2 = 0.76$).



444 **Figure 8.** Correlation between peak groundwater level (PGL) and lag time of the delayed
445 streamflow peak (t_{2p}). The insert shows the same plot with linear fitting. Orange solid circles
446 represent hybrid bimodal events.
447

448 Moreover, as shown in Figure 9, q_s also has a strong linear relationship with groundwater
449 level ($q_s = -10 \times PGL + 94.8$, $R^2 = 0.91$, $p < 0.01$). These results highlight the significant influence

450 of groundwater on flood generation in the studied watershed, suggesting that incorporating
451 groundwater level variations into flood forecasting models could enhance their accuracy.



452

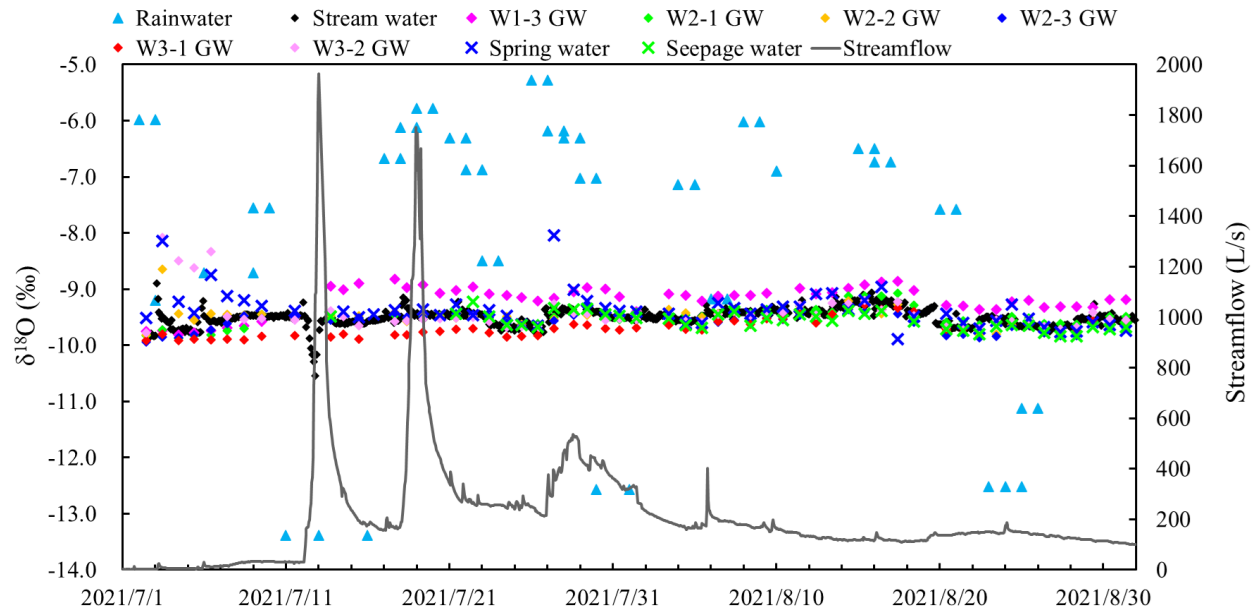
453 **Figure 9.** Correlation between mean groundwater (MGL/PGL) level and stormflow amount (q_s)
454 for bimodal events. Orange stars represent hybrid bimodal events.

455 For both fitted lines, the closely matching fitting lines for hybrid bimodal events support the
456 hypothesis that these high, delayed streamflow responses, which may appear unimodal, are, in fact,
457 bimodal. During hybrid bimodal events, the delayed peak increased rapidly and reached its peak
458 within one day, practically merging with the direct peak. This led to a potentially misleading result
459 that only one peak was generated. This occurrence was likely due to the groundwater level rising
460 rapidly to a critical level with substantially higher hydraulic conductivity, allowing a larger portion
461 of the hillslope to become hydraulically connected to the stream during these events within a very
462 short time. Consequently, a substantial amount of groundwater was quickly discharged into the
463 channel.

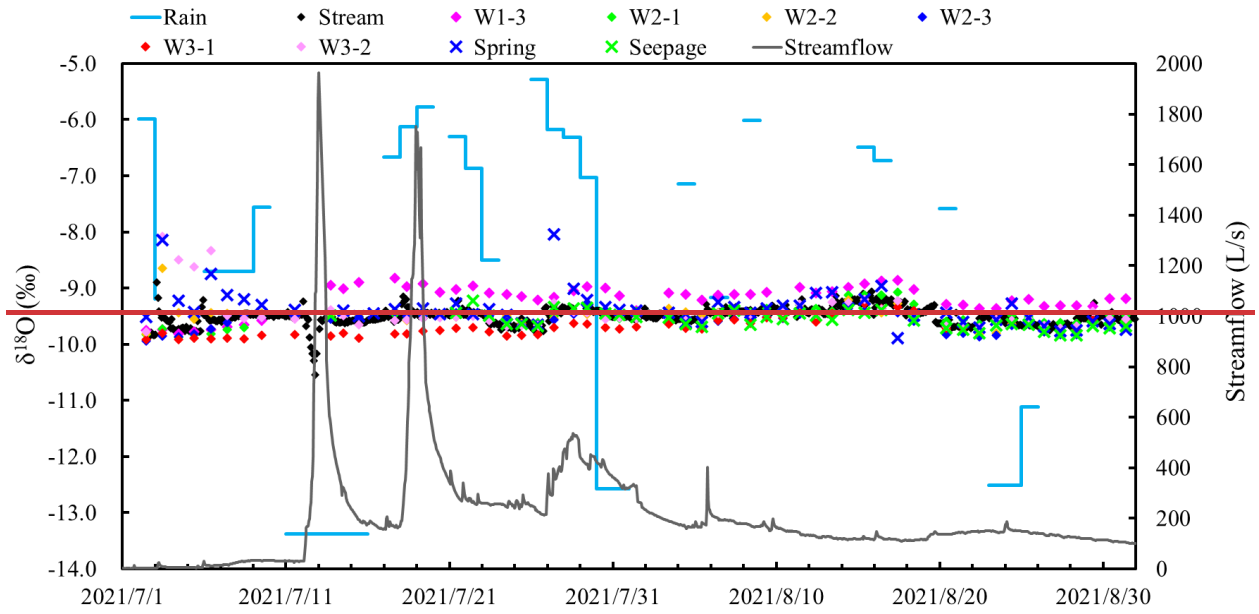
464 3.5 Isotope composition of groundwater and stream water

465 To gain additional insight into the control of groundwater level on delayed stormflow, the
466 isotope compositions of different water bodies were analyzed. Figure 10 summarizes the $\delta^{18}\text{O}$ of
467 stream, spring, seepage water and the groundwater $\delta^{18}\text{O}$ from all boreholes between July 1 and

468 September 1 in 2021. Rainwater exhibited a high variation in $\delta^{18}\text{O}$ composition (ranging from -
469 14.42 to -5.28 ‰), with a rainfall-weighted mean $\delta^{18}\text{O}$ value of -9.197. In contrast, groundwater
470 $\delta^{18}\text{O}$ composition appeared more stable throughout the sampling period, showing little variation
471 across various boreholes, with a mean $\delta^{18}\text{O}$ value ranging from -9.76 ± 0.10 to -9.08 ± 0.86 ‰. This
472 stability indicates minimal event-based mixing with rainwater. The $\delta^{18}\text{O}$ values of spring and
473 seepage water followed a pattern similar to that of groundwater. The average $\delta^{18}\text{O}$ value of the
474 stream (-9.51‰) closely resembled that of groundwater (-9.49‰). Although the stream's $\delta^{18}\text{O}$
475 composition briefly deviated toward that of rainfall during a storm, it quickly reverted to its
476 previous value, resembling groundwater. Large isotopic variation in rainfall was dampened in the
477 stream, indicating that both baseflow and some stormflow originated from groundwater storage
478 with a consistent isotopic ratio, a result of dispersion and mixing processes.



479



480

481

482

Figure. 10. Stable isotope $\delta^{18}\text{O}$ time series of rainfall-rainwater, streamflow-stream water and groundwater.

483

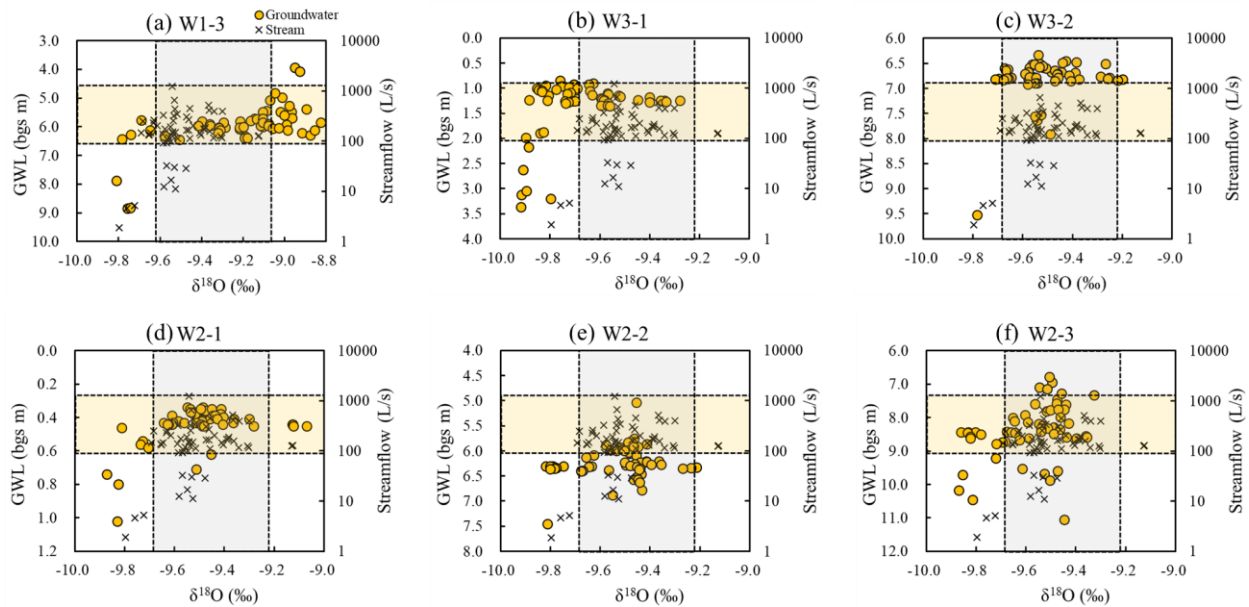
484

485

486

In Figure 11, groundwater $\delta^{18}\text{O}$ values were plotted against groundwater levels for each borehole, and stream water $\delta^{18}\text{O}$ values were plotted against streamflow. The variability of groundwater $\delta^{18}\text{O}$ increased with rising groundwater levels, suggesting a stronger influence of rainwater on groundwater. Stream water's $\delta^{18}\text{O}$ remained independent of streamflow volume and

487 exhibited a range of variation similar to that of groundwater. Notably, the overlapping isotopic
 488 compositions, including those during stormflow, were predominantly found in regions with higher
 489 groundwater levels. This observation underscores that, even during stormflow events, groundwater
 490 remains the primary source of streamflow.



491
 492 **Figure 11.** $\delta^{18}\text{O}$ measurements in groundwater and stream water from July 1 to September 1, 2021.
 493 Circles and cross represent the $\delta^{18}\text{O}$ of groundwater and stream water, respectively.

494 **4. Discussion**

495 **4.1 Lag time of delayed streamflow peaks**

496 The lag time of delayed peaks varies across different water sources, providing valuable
 497 insights for estimating stormflow water resources. Haga *et al.* (2005) conducted relevant studies
 498 in a forested unchanneled catchment, noting that events with shorter lag times (<2 hours)
 499 predominantly exhibited runoff composed of saturation excess overland flow near the spring area.
 500 In contrast, events with longer lag times (>24 hours) were characterized by river runoff mainly
 501 composed of saturated subsurface flow above the soil-bedrock interface. Becker (2005)

502 synthesized lag times from various studies in different basins, observing a trend where lag times
503 for the three main flow components differed by at least one order of magnitude, following the
504 pattern overland flow < subsurface flow < baseflow. This substantial difference in lag times is
505 likely attributed to the stochastic triggering of different flow paths by rainfall forcing in distinct
506 events.

~~507 Lag times of the direct streamflow peaks for both unimodal and bimodal events were
508 generally within 30 min in this study, which had no significant correlation with rainfall amount,
509 rainfall intensity, or pre-event streamflow with the correlation coefficients were 0.005, 0.017 and
510 0.012, respectively, indicating the direct streamflow peak was nearly concurrent with the rainfall.
511 Therefore, we could infer that the direct peaks were generated by bypass flow via macropores,
512 fractures or soil-bedrock interface (Buttle and Turcotte, 1999; Onda *et al.*, 2001; Uchida *et al.*,
513 2005; Xu *et al.*, 2016), or contributed by the direct rainfall into the channel considering that 1 h
514 was roughly the routing time of river network in XEW (Zhao *et al.*, 2019).~~

515 Lag times for the direct streamflow peaks, observed in both unimodal and bimodal events in
516 this study, were generally within 30 minutes. These lag times exhibited no significant correlation
517 with rainfall amount, rainfall intensity, or pre-event streamflow (correlation coefficients of 0.005,
518 0.017, and 0.012, respectively). This lack of correlation suggests that the direct streamflow peaks
519 were nearly concurrent with rainfall. Therefore, we infer that these direct peaks were generated
520 either through bypass flow mechanisms, such as macropores, fractures, or soil-bedrock interfaces,
521 as interpreted in Buttle and Turcotte (1999), Onda *et al.* (2001), Uchida *et al.* (2005), and Xu *et al.*
522 (2016). Alternatively, they could have been directly contributed to the channel by rainfall. This
523 interpretation aligns with the consideration that the routing time of the river network in XEW is
524 approximately 1 hour (Zhao *et al.*, 2019).

525 In contrast to the direct peaks, the time lags from the peak rainfalls to the delayed peaks were
 526 considerably longer, ranging from 5 hours to 9.9 days (Figure 3). This lag time in our study aligns
 527 with findings from other studies where similar parameters were calculated (refer to Table 3). The
 528 results imply that the delayed peaks observed in XEW were likely generated by subsurface flow
 529 processes, as indicated in the work of Lischeid *et al.* (2002).

530 **Table 3.** Lag time between peak rainfall intensity and the delayed streamflow peak in this study
 531 and in previous studies.

<u>Reference</u>	<u>Lag time of delayed peak</u>	<u>The source of the delayed peak</u>
<u>Anderson & Burt (1978)</u>	<u>About one day</u>	<u>Subsurface flow</u>
<u>Onda <i>et al.</i> (2001)</u>	<u>Ten hours to one week</u>	<u>Subsurface flow and bedrock groundwater</u>
<u>Masiyandima <i>et al.</i> (2003)</u>	<u>Several hours</u>	<u>Subsurface flow</u>
<u>Becker (2005)</u>	<u>A day to several weeks</u>	<u>Subsurface stormflow</u>
<u>Zillgens <i>et al.</i> (2007)</u>	<u>Three to five days</u>	<u>Subsurface flow</u>
<u>Birkinshaw (2008)</u>	<u>Several tens of hours to a few days</u>	<u>Subsurface stormflow</u>
<u>Kosugi <i>et al.</i> (2011)</u>	<u>Two to three days</u>	<u>Bedrock groundwater</u>
<u>Fencia <i>et al.</i> (2014)</u>	<u>Several hours or days</u>	<u>Subsurface flow</u>
<u>Padilla <i>et al.</i> (2014, 2015)</u>	<u>Within four days</u>	<u>Bedrock groundwater</u>
<u>Yang <i>et al.</i> (2015)</u>	<u>Several hours</u>	<u>Subsurface flow</u>
<u>This study</u>	<u>5 hours to 9.9 days</u>	<u>Subsurface flow (groundwater flow)</u>
<u>Reference</u>	<u>Lag-time-of-delayed-peak</u>	<u>The-source-of-the-delayed-peak</u>
<u>Onda <i>et al.</i> (2001)</u>	<u>Ten-hours-to-one-week</u>	<u>Subsurface-flow-and-bedrock-groundwater</u>
<u>Zillgens <i>et al.</i> (2007)</u>	<u>Three-to-five-days</u>	<u>Subsurface-flow</u>

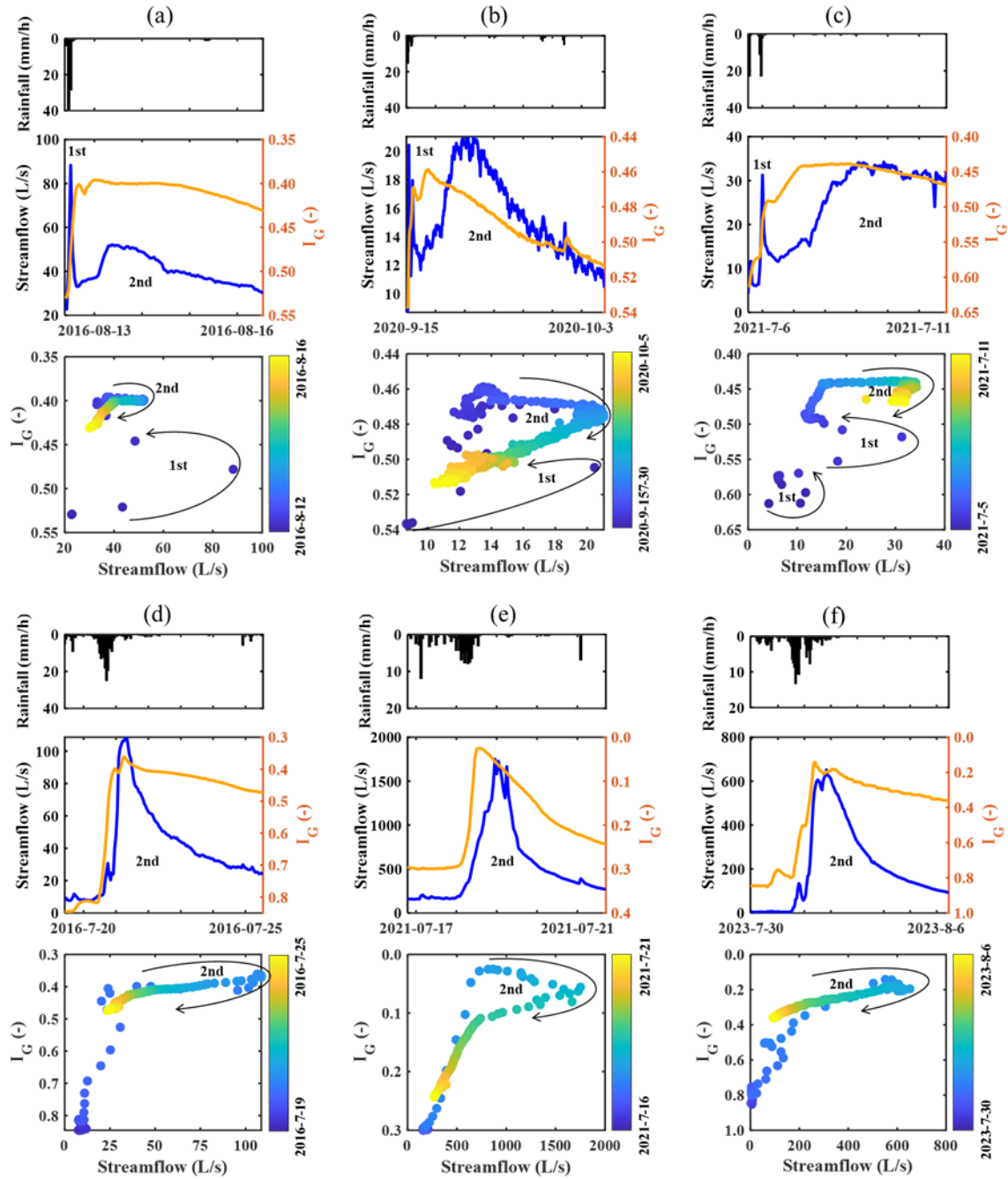
Padilla <i>et al.</i> (2014, 2015)	Within four days	Bedrock groundwater
Masiyandima <i>et al.</i> (2003)	Several hours	Subsurface flow
Anderson & Burt (1978)	About one day	Subsurface flow
This study	5 hours to 9.9 days	Subsurface flow (groundwater flow)

532

533 4.2 Hysteresis between groundwater level and streamflow

534 For bimodal events in XEW, the non-linear relationship between groundwater level and
535 streamflow results in hysteretic relationships between the two variables. Figure ~~11~~12 shows time
536 series for streamflow and I_G as well as scatter plots comparing the two variables for the six events
537 used in section 3.3. As noted by Dunne (1978), when two runoff peaks appeared in an event, there
538 must be at least two zones in the catchment that responded to the storm and contributed to runoff.
539 The hysteretic nature highlights the possibility of multiple hydrological compartments being active
540 and these compartments are not necessarily contributing significant flows simultaneously but
541 rather sequentially during the runoff generation period (Fovet *et al.*, 2015; Martínez-Carreras *et*
542 *al.*, 2016).

543



544
 545 **Figure H12.** Streamflow and I_G with corresponding scatter plots between both variables for three
 546 typical bimodal and three hybrid bimodal events. Note that the axis scales vary between events.
 547 Arrows indicate progression of time. Direct peaks in bimodal hydrographs indicated as “1st” and
 548 delayed peaks as “2nd”.

549

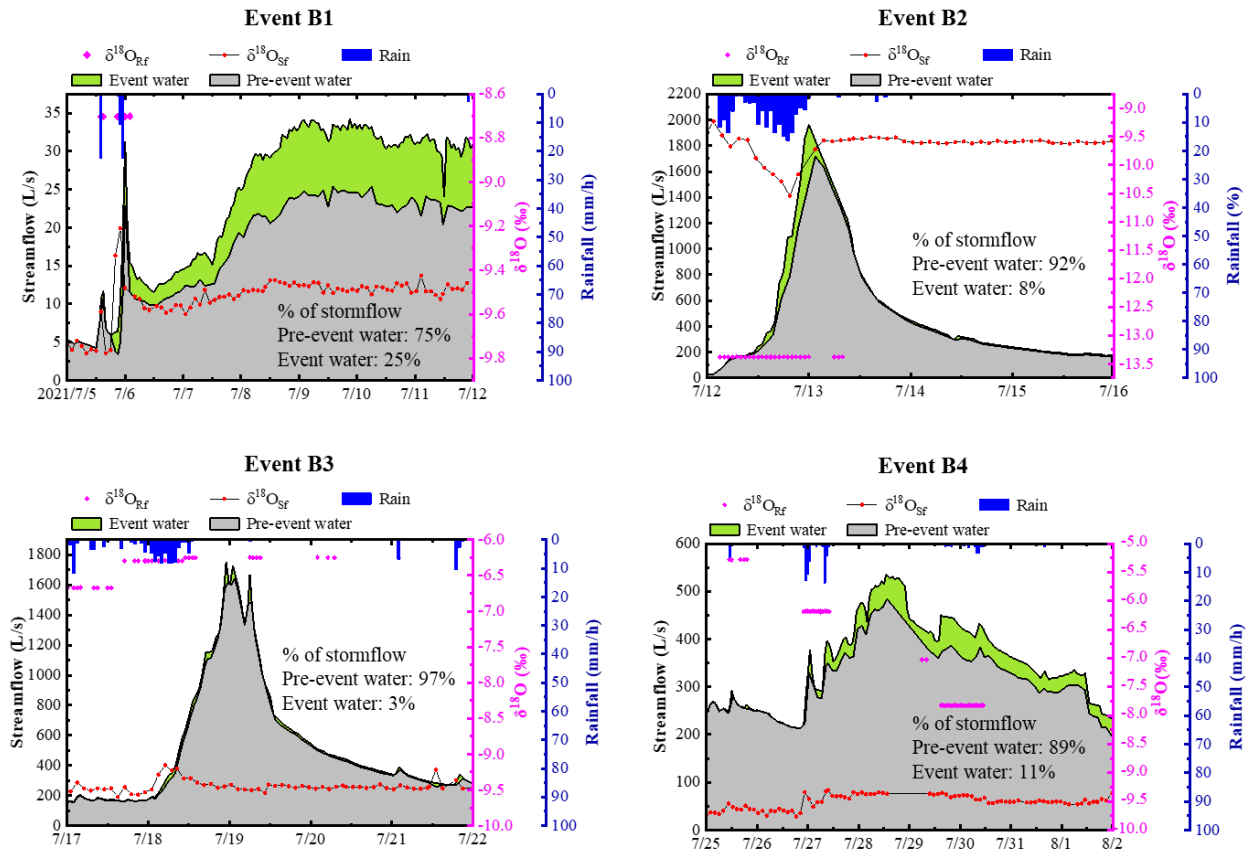
550 Streamflow increased quickly and peaked before groundwater level during direct peaks,
551 resulting in an anti-clockwise hysteretic loop. It can be explained that direct peaks were formed by
552 rainfall directly falling onto the channel or a saturation zone near the channel, and/or by the flow
553 that contributed to the channel through rapid routes, as observed in other watersheds by Jackisch
554 *et al.* (2016). In contrast, groundwater level peaked first during delayed peaks, indicating that the
555 groundwater level in the watershed peaked first and subsequently released water, creating the
556 delayed runoff peak. This behavior may be attributed to the groundwater level surpassing a
557 threshold for generating bimodal hydrographs, leading to enhanced hydraulic connectivity
558 between hillslopes and the channel. This, in turn, resulted in the swift release of a substantial
559 amount of groundwater or subsurface flow (Burt & Butcher, 1985; Detty and McGuire, 2010;
560 McGlynn & McDonnell, 2003; McGuire and McDonnell, 2010; Scaife and Band, 2017).
561 Consequently, the groundwater level is not merely a passive feature in this watershed, where
562 shallow groundwater may constitute the primary runoff component, but actively controls the
563 stormflow.

564 **4.3 Two-component hydrograph separation**

565 The two-component hydrograph separation was performed for four bimodal storm events
566 using the $\delta^{18}\text{O}$ of the bulk rainfall, a pre-event water signature (represented by the stream $\delta^{18}\text{O}$
567 before the rainfall) and the monitored stream water signature during the events. These four events
568 were chosen because their relatively complete isotope data. It should be noted that in all four
569 rainfall events, $\delta^{18}\text{O}$ values in rain and stream water were notably different, which is a requirement
570 for end-member hydrograph separation analysis. The hydrograph separation results, as well as the
571 $\delta^{18}\text{O}$ series of rainwater and stream water were shown in Figure ~~12~~13.

572 Regarding the water sources separation result, these four events can be divided into two
573 groups: Event B1 and B4, the major stormflow process were lagged and considerably damped, and
574 event water contributions were higher compared to the other two events. The fraction of event
575 water comprising the hydrograph was 25% in Event B1, and the contribution ratio of event water
576 in Event 4 was 11%. Considering that the rain had already stopped, the event water component of
577 the delayed peak should be the rainwater temporarily stored in the watershed during the rainfall
578 process. Event B2 and especially Event B3, however, were almost entirely pre-event water
579 dominated (the contributions of pre-event water were 92% for Event 2 and 97% for Event B3),
580 although it was evident that some event water contributed to the stormflow during the rising and
581 peak period of streamflow, this water may have originated from the direct rainfall or rain water
582 taking a rapid route to the stream channel.

583 The hydrograph separation results indicated that the streamflow contribution of pre-event
584 water changed virtually in sync with streamflow following the onset of rain, almost entirely
585 dominating the hydrograph, while event water dominated the sharp streamflow peak responding
586 to high-intensity storm. Early in the rainy event, the pre-event component of the hydrograph
587 exceeded 50%, indicating a sufficiently swift groundwater response such that considerable
588 amounts of groundwater were released soon after the start of rain.



589
 590 **Figure 1213.** The partitioning of stormflow into its pre-event and event water sources using one-
 591 tracer two component hydrograph separation analysis with $\delta^{18}\text{O}$ as tracer for the four storm
 592 events. $\delta^{18}\text{O}_{\text{Rf}}$ and $\delta^{18}\text{O}_{\text{Sf}}$ are the $\delta^{18}\text{O}$ respectively for rain and stream water.

593 In addition, there was a noticeable, gradual rise in the pre-event water contribution to total
 594 stormflow as the catchment was wetting-up (Figure 1213). Event B1 had a rather dry antecedent
 595 condition and showed a relatively lower pre-event water percentage (about 75%). Event 3 in the
 596 temporal sequence had a extremely high pre-event water proportion (approximately 97%) and
 597 occurred under highly wet antecedent conditions. In Event B4, due to a little reduced wetness
 598 condition compared to the preceding Event B3, the percentage of pre-event water decreased
 599 somewhat to approximately 89%. This pattern may be attributed to increased water flux during the
 600 wetting-up process when the water table rose into near surface soil layers with high saturated
 601 hydraulic conductivity. The rate of groundwater increase slowed as a result of the higher

602 transmissivity, and more pre-event water was mobilized and travelled rapidly to the stream via
603 shallow flow pathways (Lundin, 1982).

604 4.4 Filed observation

605 Our field observations on-site indicate that direct exfiltration of groundwater into the runoff
606 predominates, with few signs of hillslope overland flow. For example, during a heavy storm on
607 July 5, 2021, characterized by short duration (7 hours) and very high intensity (27.6 mm/h) with a
608 total rainfall of 65.2 mm, minimal overland flow was observed at the study site. However, post the
609 storm on July 5, the spring water flow from Hillslope 2 substantially increased. Moreover, at
610 various points in the watershed, seepage flow was observed gushing from fractures in the stone
611 and holes in the earth. These field observations strongly suggest the direct exfiltration of
612 groundwater into the runoff, providing further support to the notion that groundwater significantly
613 contributes to stormflow in the watershed.



614
615 **Figure 14.** Field observations of the spring and the seepage flows. HS1, HS2 and HS3 are Hillslope
616 1, Hillslope 2 and Hillslope 3, respectively.

617 5. Conclusions

618 Based on observations from 2013 to 2023, the study carried out an event-scale analysis of
619 streamflow hydrographs in a semi-humid forested watershed of North China. Three stormflow

620 patterns with distinct shaped hydrograph, i.e., unimodal, bimodal, and hybrid bimodal were
621 identified. Particularly, their rainfall-runoff response characteristics as well the stormflow
622 composition were analyzed, and derived the following conclusions:

623 1) Direct peaks for both unimodal and bimodal events occurred within 1 hour following the
624 peak rainfall, while the lag time of delayed peaks ranged between 5 h and 9.9 days. The stormflow
625 amount generated by bimodal events, due to the delayed peak, was several to hundreds of times
626 more than that of the unimodal events, often resulting in flooding.

627 2) Delayed stormflow appeared when the sum of event rainfall amount (P) and antecedent
628 soil moisture index (ASI) exceeding 200 mm. Stormflow yield is positively proportional to event
629 peak groundwater level while the lag time of delayed peak showed an inverse correlation with
630 peak groundwater level.

631 3) The isotopic analysis and two-component hydrograph separation unveiled that pre-event
632 water predominantly contributed to the delayed stormflow, with event water dominating the sharp
633 streamflow peak in response to high-intensity storms.

634 4) Streamflow peaked before groundwater level during direct peaks, suggesting that direct
635 streamflow peaks are from direct rainfall onto the channel or rapid flow through macropores and
636 bedrock fractures, Discharge peaked before catchment storage during single peak. But
637 groundwater levels peaked first during delayed streamflow, suggested that the delayed stormflow
638 is primarily made up of shallow groundwater, and this is further supported by field observation.

639 This study clarified the prerequisites for bimodal stormflow, and the provided information on
640 the response characteristics and water resources of stormflow is not common knowledge for
641 regions. We believe these findings can enrich runoff generation theory and contribute new insights
642 for stormflow modelling in other similar regions.

643 **Data availability**

644 All the data used in this study will be available at the Zenodo website at the time of
645 publication.

646 **Author contribution**

647 ZC contributed the conceptualization, formal analysis, investigation and writing; FT
648 contributed the conceptualization, formal analysis and revision; ZZ, ZX, YD and JW contributed
649 the Investigation; M contributed the writing.

650 **Competing interests**

651 Some authors are members of the editorial board of Hydrology and Earth System Sciences.

652 **Financial support**

653 This study was supported by the National Key R&D Program of China (2022YFC3002902)
654 and the National Natural Science Foundation of China (51825902).

655 **Acknowledgments**

656 We acknowledge Jeffrey McDonnell for constructive advice on this study.

657 **References**

658 Ali, G., Tetzlaff, D., McDonnell, J. J., Soulsby, C., Carey, S., Laudon, H., McGuire, K., Buttle, J., Seibert, J.,
659 Shanley, J. (2015). Comparison of threshold hydrologic response across northern catchments. *Hydrological*
660 *Process*, 29 (16), 3575–3591. <https://doi.org/10.1002/hyp.10527>

661 Anderson, M. G., & Burt, T. P. (1977). Automatic monitoring of soil moisture conditions in a hillslope spur and
662 hollow. *Journal of Hydrology*, 33(1–2), 0–36. [https://doi.org/10.1016/0022-1694\(77\)90096-8](https://doi.org/10.1016/0022-1694(77)90096-8)

663 Anderson, M. G., & Burt, T. R. (1978). The role of topography in controlling throughflow generation. *Earth*
664 *Surface Processes*, 3(4), 331–334. <https://doi.org/10.1002/esp.3290030402>

665 Becker, A. (2005). Runoff Processes in Mountain Headwater Catchments: Recent Understanding and Research
666 Challenges. *Global Change and Mountain Regions*, 283–295. https://doi.org/10.1007/1-4020-3508-x_29

667 Becker, A., & McDonnell, J. J. (1998). Topographical and ecological controls of runoff generation and lateral
668 flows in mountain catchments. *IAHS Publications-Series of Proceedings and Reports-Intern Assoc*
669 *Hydrological Sciences*, 248, 199-206.

670 [Birkinshaw, S. J. \(2008\). Physically-based modelling of double-peak discharge responses at Slapton Wood](#)
671 [catchment. *Hydrological Processes: An International Journal*, 22\(10\), 1419–1430. \[https://doi.org/10.1002/\]\(https://doi.org/10.1002/hyp.6694\)](#)
672 [hyp.6694](#)

673 Burt, T. P., & Butcher, D. P. (1985). Topographic controls of soil moisture distributions. *Journal of Soil Science*,
674 36(3), 469–486. <https://doi.org/10.1111/j.1365-2389.1985.tb00351.x>

675 Buttle, J. M., Dillon, P. J., & Eerkes, G. R. (2004). Hydrologic coupling of slopes, riparian zones and streams:
676 An example from the Canadian Shield, *Journal of Hydrology*, 287(1–4), 161–177. [https://doi.org/10.1016/](https://doi.org/10.1016/j.jhydrol.2003.09.022)
677 [j.jhydrol.2003.09.022](#)

678 Buttle, J. M., & Turcotte, D. S. (1999). Runoff processes on a forested slope on the Canadian Shield. *Hydrology*
679 *Research*, 30(1), 1-20. [https://doi.org/10.1016/S0304-2995\(99\)80027-8](https://doi.org/10.1016/S0304-2995(99)80027-8)

680 Detty, J. M., & McGuire, R. J. (2010). Threshold changes in storm runoff generation at a till-mantled headwater
681 catchment. *Water Resources Research*, 46(7), 759–768. <https://doi.org/10.1029/2009wr008102>

682 Dingman, S. L. (2015). *Physical hydrology*. Long Grove, IL: Waveland Press.

683 Dubreuil, P. L. (1960). Etude hydrologique de petits bassins en Cote d’Ivoire. Rapport general. ORSTOM
684 Service Hydrologique.

685 Dubreuil, P. L. (1985). Review of field observations of runoff generation in the tropics. *Journal of Hydrology*,
686 80(3-4), 237–264. [https://doi.org/10.1016/0022-1694\(85\)90119-2](https://doi.org/10.1016/0022-1694(85)90119-2)

- 687 Dunne, T. (1978). Field studies of hillslope flow processes. In M. J. Kirkby (Eds.), Hillslope Hydrology (pp.
688 227–293). London, Wiley.
- 689 [Fenicia, F., Kavetski, D., Savenije, H. H., Clark, M. P., Schoups, G., Pfister, L., & Freer, J. \(2014\). Catchment](#)
690 [properties, function, and conceptual model representation: is there a correspondence?. *Hydrological*](#)
691 [Processes, 28\(4\), 2451-2467. <https://doi.org/10.1002/hyp.9726>](#)
- 692 Fovet, O., Ruiz, L., Hrachowitz, M., Faucheux, M., & Gascuel-Oudou, C. (2015). Hydrological hysteresis and
693 its value for assessing process consistency in catchment conceptual models. *Hydrology and Earth System*
694 *Sciences, 19(1)*, 105-123. <https://doi.org/10.5194/hess-19-105-2015>
- 695 Fu, C., Chen, J., Jiang, H., & Dong, L. (2013). Threshold behavior in a fissured granitic catchment in southern
696 China: 1. Analysis of field monitoring results. *Water Resources Research, 49(5)*, 2519–2535.
697 <https://doi.org/10.1002/wrcr.20191>
- 698 Graeff, T., Zehe, E., Reusser, D., Lück, E., Schröder, B., Wenk, G., John, H., & Bronstert, A. (2009). Process
699 identification through rejection of model structures in a mid-mountainous rural catchment: observations of
700 rainfall-runoff response, geophysical conditions and model inter-comparison. *Hydrological Processes,*
701 *23(5)*, 702–718. <https://doi.org/10.1002/hyp.7171>
- 702 Gu, W. (1996). On the hydrograph separation traced by environmental isotopes. *Advances in Water Science,*
703 *7(2)*: 105–111.
- 704 Haga, H., Matsumoto, Y., Matsutani, J., Fujita, M., Nishida, K., & Sakamoto, Y. (2005). Flow paths, rainfall
705 properties, and antecedent soil moisture controlling lags to peak discharge in a granitic unchanneled
706 catchment. *Water Resources Research, 41(12)*, 2179–2187. <https://doi.org/10.1029/2005wr004236>
- 707 Iwagami, S., Tsujimura, M., Onda, Y., Shimada, J., & Tanaka, T. (2010). Role of bedrock groundwater in the
708 rainfall-runoff process in a small headwater catchment underlain by volcanic rock. *Hydrological Processes,*
709 *24(19)*, 2771–2783. <https://doi.org/10.1002/hyp.7690>
- 710 Jackisch, C., Angermann, L., Allroggen, N., Sprenger, M., Blume, T., Weiler, M., Tronicke, J., & Zehe, E.
711 (2016). In situ investigation of rapid subsurface flow: identification of relevant spatial structures beyond

712 heterogeneity. *Hydrology and Earth System Sciences Discussions*, 1–32. <https://doi.org/10.5194/hess->
713 2016-190

714 Jenkins, A., Ferrier, R. C., Harriman, R., & Ogunkoya, Y. O. (1994). A case study in catchment hydrochemistry:
715 Conflicting interpretations from hydrological and chemical observations, *Hydrological Processes*, 8(4),
716 335–349. <https://doi.org/10.1002/hyp.3360080406>

717 Kosugi, K., Fujimoto, M., Katsura, S., Kato, H., Sando, Y., & Mizuyama, T. (2011). Localized bedrock aquifer
718 distribution explains discharge from a headwater catchment. *Water Resources Research*, 47(7).
719 <https://doi.org/1029/2010WR009884>

720 Lischeid, G., Kolb, A., & Alewell, C. (2002). Apparent translatory flow in groundwater recharge and runoff
721 generation. *Journal of Hydrology*, 265(1–4), 195–211. [https://doi.org/10.1016/s0022-1694\(02\)00108-7](https://doi.org/10.1016/s0022-1694(02)00108-7)

722 Lundin L. (1982) Soil moisture and ground water in till soil and the significance of soil type for runoff. PhD
723 Thesis, Uppsala University, UNGI Report, 56, 216.

724 Martínez-Carreras, N., Hissler, C., Gourdol, L., Klaus, J., Juilleret, J., Iffly, J. F., & Pfisteret, L. (2016). Storage
725 controls on the generation of double peak hydrographs in a forested headwater catchment. *Journal of*
726 *Hydrology*, 543, 255–269. <https://doi.org/10.1016/j.jhydrol.2016.10.004>

727 Martínez-Carreras, N., Wetzel, C. E., Frentress, J., Ector, L., McDonnell, J. J., Hoffmann, L., Pfister, L., 2015.
728 Hydrological connectivity inferred from diatom transport through the riparian-stream system. *Hydrology and*
729 *Earth System Sciences*, 19(7), 3133–3151. <https://doi.org/10.5194/hess-19-3133-2015>

730 Masiyandima, M. C., van de Giesen, N., Diatta, S., Windmeijer, P. N., & Steenhuis, T. S. (2003). The hydrology
731 of inland valleys in the sub-humid zone of West Africa: rainfall-runoff processes in the M’be experimental
732 watershed. *Hydrological Processes*, 17(6), 1213–1225. <https://doi:10.1002/hyp.1191>

733 McDonnell, J. J., Bonell, M., Stewart, M. K., & Pearce, A. J. (1990). Deuterium variations in storm rainfall:
734 Implications for stream hydrograph separation. *Water resources research*, 26(3), 455-458.
735 <https://doi.org/10.1029/WR026i003p00455>

736 McDonnell, J. J., Sivapalan, M., Vaché, K., Dunn, S., Grant, G., Haggerty, R., Hinz, C., Hooper, R., Kirchner,
737 J., Roderick, M. L., Selker, J., Weiler, M. (2007). Moving beyond heterogeneity and process complexity:

738 A new vision for watershed hydrology. *Water Resources Research*, 43(7). [https://doi.org/10.1029/](https://doi.org/10.1029/2006WR005467)
739 2006WR005467

740 McGlynn, B. L., & McDonnell, J. J. (2003). Quantifying the relative contributions of riparian and hillslope zones
741 to catchment runoff, *Water Resources Research*, 39(11), 1310. <https://doi.org/10.1029/2003wr002091>

742 McGuire, K. J., & McDonnell, J. J. (2010). Hydrological connectivity of hillslopes and streams: Characteristic
743 time scales and nonlinearities. *Water Resources Research*, 46(10). <https://doi.org/10.1029/2010WR009341>

744 Mosley, M. P. (1979). Streamflow generation in a forested watershed, New Zealand. *Water Resources Research*,
745 15(4), 795–806. <https://doi.org/10.1029/wr015i004p00795>

746 Onda, Y., Komatsu, Y., Tsujimura, M., & Fujihara, J. (2001). The role of subsurface runoff through bedrock on
747 storm flow generation. *Hydrological Processes*, 15(10), 1693–1706. <https://doi.org/10.1002/hyp.234>

748 Padilla, C., Onda, Y., Iida, T., Takahashi, S., & Uchida, T. (2014). Characterization of the groundwater response
749 to rainfall on a hillslope with fractured bedrock by creep deformation and its implication for the generation
750 of deep-seated landslides on Mt. Wanitsuka, Kyushu Island. *Geomorphology*, 204, 444–458.
751 <https://doi.org/10.1016/j.geomorph.2013.08.024>

752 Padilla, C., Onda, Y., & Iida, T. (2015). Interaction between runoff-bedrock groundwater in a steep headwater
753 catchment underlain by sedimentary bedrock fractured by gravitational deformation. *Hydrological*
754 *Processes*, 29(20), 4398–4412. <https://doi.org/10.1002/hyp.10498>

755 Penna, D., Tromp-van Meerveld, H. J., Gobbi, A., Borga, M., & Dalla Fontana, G. (2011). The influence of soil
756 moisture on threshold runoff generation processes in an alpine headwater catchment. *Hydrology and Earth*
757 *System Sciences*, 15(3), 689–702. <https://doi.org/10.5194/hess-15-689-2011>

758 Phillips, J. D. (2003). Sources of nonlinearity and complexity in geomorphic systems, *Progress in Physical*
759 *Geography*, 27(1), 1–23. <https://doi.org/10.1191/0309133303pp340ra>

760 Powell, D. N., Khan, A. A., Aziz, N. M., & Raiford, J. P. (2007). Dimensionless rainfall patterns for South
761 Carolina. *Journal of Hydrologic Engineering*, 12(1), 130–133. [https://doi.org/10.1061/\(asce\)1084-](https://doi.org/10.1061/(asce)1084-0699(2007)12:1(130))
762 0699(2007)12:1(130)

763 Ross, C. A., Ali, G. A., Spence, C., & Courchesne, F. (2021). Evaluating the Ubiquity of Thresholds in
764 Rainfall - Runoff Response Across Contrasting Environments. *Water Resources Research*, *57*(1),
765 e2020WR027498. <https://doi.org/10.1029/2020wr027498>

766 Scaife, C. I., & Band, L. E. (2017). Nonstationarity in threshold response of stormflow in southern Appalachian
767 headwater catchments. *Water Resources Research*, *53*(8), 6579–6596. [https://doi.org/10.1002/](https://doi.org/10.1002/2017WR020376)
768 2017WR020376

769 Sivapalan, M. (2003), Process complexity at hillslope scale, process simplicity at the watershed scale: Is there a
770 connection? *Hydrol. Processes*, *17*(5), 1037–1041. <https://doi:10.1002/hyp.5109>.

771 [Sloto, R. A., & Crouse, M. Y. \(1996\). HYSEP: A computer program for streamflow hydrograph separation and](https://doi.org/10.3133/wri964040)
772 [analysis \(No. 96-4040\). US Geological Survey. https://doi.org/10.3133/wri964040](https://doi.org/10.3133/wri964040)

773 Tian, F., Li, H., & Sivapalan, M. (2012). Model diagnostic analysis of seasonal switching of runoff generation
774 mechanisms in the blue river basin, oklahoma. *Journal of Hydrology*, *418–419*, 136–149.
775 <https://doi.org/10.1016/j.jhydrol.2010.03.011>

776 Tie, Q., Hu, H., Tian, F., Guan, H., & Lin, H. (2017). Environmental and physiological controls on sap flow in
777 a subhumid mountainous catchment in north china. *Agricultural and Forest Meteorology*, *240–241*, 46–57.
778 <https://doi.org/10.1016/j.agrformet.2017.03.018>

779 Tromp-van Meerveld, H. J., & McDonnell, J. J. (2006), Threshold relations in subsurface stormflow: 1. A 147-
780 storm analysis of the Panola hillslope. *Water Resources Research*, *42*, W02410. [https://doi.org/10.1029/](https://doi.org/10.1029/2004WR003778)
781 2004WR003778

782 Uchida, T., Tromp-van Meerveld, I., & McDonnell, J. J. (2005). The role of lateral pipe flow in hillslope runoff
783 response: An intercomparison of non-linear hillslope response. *Journal of Hydrology*, *311*(1-4), 117–133.
784 <https://doi.org/10.1016/j.jhydrol.2005.01.012>

785 Westhoff, M. C., Bogaard, T. A., & Savenije, H. H. G. (2011). Quantifying spatial and temporal discharge
786 dynamics of an event in a first order stream, using distributed temperature sensing. *Hydrology and Earth*
787 *System Sciences*, *15*(6), 1945-1957. <https://doi.org/10.5194/hess-15-1945-2011>

788 Weyman, D., R. (1970). Throughflow on hillslopes and its relation to the stream hydrograph. International
789 Association of Scientific Hydrology. *Bulletin*, 15(3), 25–33. <https://doi.org/10.1080/02626667009493969>

790 Wrede, S., Fenicia, F., Martínez-Carreras, N., Juilleret, J., Hissler, C., Krein, A., Savenije, H. H. G., Uhlenbrook,
791 S., Kavetski, D., Pfister, L. (2015). Towards more systematic perceptual model development: a case study
792 using 3 Luxembourgish catchments. *Hydrological Processes*, 29(12), 2731-2750.
793 <https://doi.org/10.1002/hyp.10393>

794 Xu, Q., Liu, H., Ran, J., Li, W., & Sun, X. (2016). Field monitoring of groundwater responses to heavy rainfalls
795 and the early warning of the Kualiangzi landslide in Sichuan Basin, southwestern China. *Landslides*, 13,
796 1555-1570. <https://doi.org/10.1007/s10346-016-0717-3>

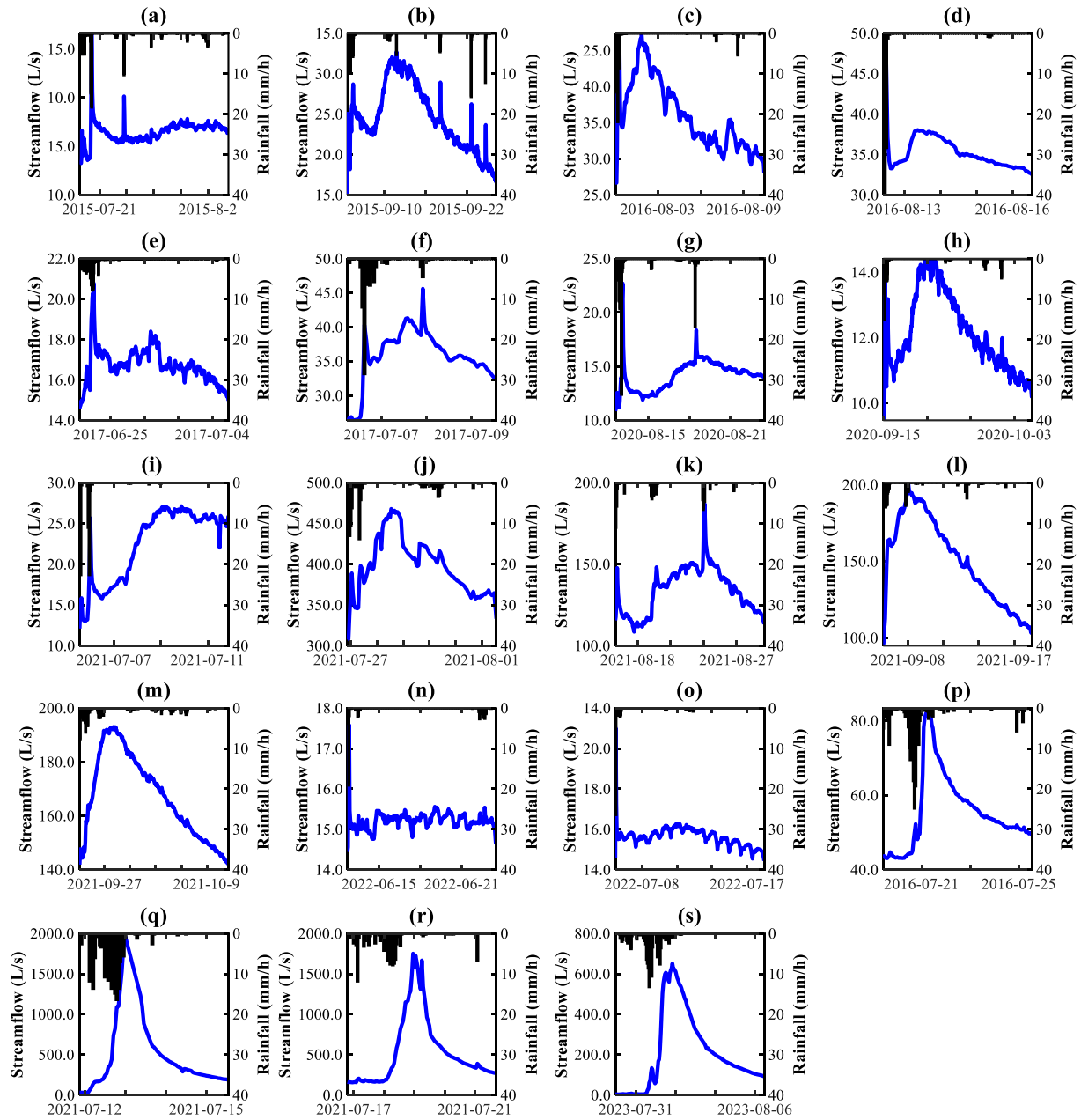
797 [Yang, Y., Endreny, T. A., & Nowak, D. J. \(2015\). Simulating double-peak hydrographs from single storms over](#)
798 [mixed-use watersheds. *Journal of hydrologic engineering*, 20\(11\), 06015003. \[https://doi.org/\]\(https://doi.org/10.1061/\(ASCE\)HE.1943-5584.0001225\)](#)
799 [10.1061/\(ASCE\)HE.1943-5584.0001225](#)

800 Zhang, G. T., Cui, P., Gualtieri, C., Zhang, J. L., Ahmed Bazai, N., Zhang, Z. T., Wang, J., Tang, J. B., Chen,
801 R., Lei, M. Y. (2021). Stormflow generation in a humid forest watershed controlled by antecedent wetness
802 and rainfall amounts. *Journal of Hydrology*, 603. <https://doi.org/10.1016/j.jhydrol.2021.127107>

803 Zillgens, B., Merz, B., Kirnbauer, R., & Tilch, N. (2007). Analysis of the runoff response of an alpine catchment
804 at different scales. *Hydrology and Earth System Sciences*, 11(4), 1441–1454. [https://doi.org/10.5194/hess-](https://doi.org/10.5194/hess-11-1441-2007)
805 [11-1441-2007](https://doi.org/10.5194/hess-11-1441-2007)

806

Appendix A: Supplementary Figures of Results and discussion



808

809

810

811

Figure A1. Rainfall and streamflow hydrograph for (a-o) 15 bimodal and (p-s) 4 hybrid bimodal events.